HHS Public Access

Author manuscript

Nat Med. Author manuscript; available in PMC 2024 June 04.

Published in final edited form as:

Nat Med. 2023 December ; 29(12): 3162–3174. doi:10.1038/s41591-023-02638-4.

Thalamic deep brain stimulation in traumatic brain injury: a phase 1, randomized feasibility study

ND Schiff[1,2,*], **JT Giacino**[3,4], **CR Butson**[5,6], **EY Choi**[7], **JL Baker**[1], **KP O'Sullivan**[5], **AP Janson**[5,8], **M Bergin**[3], **HM Bronte-Stewart**[7], **J Chua**[9], **L DeGeorge**[1], **S Dikmen**[11], **A Fogarty**[7], **LM Gerber**[9,10], **M Krel**[7], **J Maldonado**[12], **M Radovan**[13], **SA Shah**[14], **J Su**[15], **N Temkin**[16], **T Tourdias**[17], **JD Victor**[1,2], **A Waters**[3], **SA Kolakowsky-Hayner**[7], **JJ Fins**[10], **AG Machado**[18], **BK Rutt**[19,20,21], **JM Henderson**[7,20,21,*]

[1)]Feil Family Brain Mind Institute, Weill Cornell Medicine

[2)]Department of Neurology, Weill Cornell Medicine

[3)]Department of Physical Medicine and Rehabilitation, Spaulding Rehabilitation Hospital

[4)]Department of Physical Medicine and Rehabilitation, Harvard Medical School

[5)]Department of Biomedical Engineering, University of Utah

[6)]Department of Neurology, University of Florida

[*]corresponding authors.

Author Contributions

NS, JH, JG, CB, AM designed the study.

JM acted as an independent consultation-liaison psychiatrist responsible for determination of decision-making capacity for each subject prior to study enrollment.

JG, NS, LG developed study design for outcome assessment.

JG, AW, LG, JC analyzed behavioral data.

SD, NT contributed supplementary data from University of Washington study and support in the use, analysis, and interpretation of these data (Dikmen et al. 2003).

NS and JV designed and performed analysis of supplementary Dikmen et al. (2003) dataset. TT, JS, MR, BR developed the CL segmentation method.

EC, BR acquired neuroimaging data.

EC, TT, JS, MR, BR, AJ, KO, CB designed and performed analysis of neuroimaging data.

CB, AJ, KO designed and performed analysis of bioelectrical field modeling.

EC, JB, SS developed the overall study design for neurophysiological data acquisition.

EC, JB, designed cortical evoked potential experiments.

EC, JB, MK analyzed cortical evoked potential data.

LD, coordinated the study components, FDA regulatory compliance, and patient recruitment liaison with PatientWing.

JJF developed ethical framework and guidance; PI of companion BRAIN Initiative study (1RF1MH12378–01) tracking participant and family perspectives which informed subject selection and enrollment.

NS acted as administrative PI of UH3 grant.

JH acted as physician sponsor of the FDA Investigational Device Exemption (IDE) and performed all surgical implants.

HBS provided neurophysiology acquisition and interpretation during surgical implants.

NS, JH, JG, CB, BR drafted the manuscript.

All authors provided substantive feedback for revision of manuscript.

Competing Interest Statement

The following authors are listed inventors on a patent application WO2023/043786 (jointly filed by Weill Cornell Medicine, University of Utah, and Stanford University) describing detailed methods of integrating magnetic resonance imaging, biophysical modeling and electrophysiological methods for localization and placement of deep brain stimulation electrodes in the CL/DTTm of the human thalamus as described in the manuscript: Nicholas Schiff, Jonathan Baker, Christopher Butson, Andrew Janson, Kyle O'Sullivan, Jaimie Henderson, Eun Young Choi, Brian Rutt, Jason Su, Matthew Radovan. Drs. Schiff, Butson, and Baker are listed inventors on a related patent application WO2021/195062 (jointly filed by Weill Cornell Medicine, University of Utah). Drs. Schiff and Baker are listed as inventors on US Patent 9,9592,383 assigned to Weill Cornell Medicine describing different apparatus but related methods. The remaining authors declare no competing interests.

ClinicalTrials.gov identifier: NCT02881151

[7)]Department of Neurosurgery, Stanford University

[8)]Radiology and Radiological Sciences, Vanderbilt University

[9)]Department of Population Health Sciences, Weill Cornell Medicine

[10)]Department of Medicine, Weill Cornell Medicine

[11)]Department of Rehabilitation Medicine, University of Washington

[12)]Department of Psychiatry, Stanford University

[13)]Department of Computer Science, Stanford University

[14)]Department of Radiology, Weill Cornell Medicine

[15)]Department of Electrical Engineering, Stanford University

[16)]Department of Neurological Surgery, University of Washington

[17)]Department of Neuroimaging, University of Bordeaux

[18)]Neurological Institute, Cleveland Clinic

[19)]Department of Radiology, Stanford University

[20)]Wu Tsai Neurosciences Institute, Stanford University

[21)]Bio-X Program, Stanford University

Abstract

Converging evidence indicates that impairments in executive function and information processing speed limit quality of life and social reentry after moderate to severe traumatic brain injury (msTBI). These deficits reflect dysfunction of frontostriatal networks for which the central lateral (CL) nucleus of the thalamus is a critical node. The primary objective of this feasibility study was to test the safety and efficacy of deep brain stimulation within CL and the associated medial dorsal tegmental tract (CL/DTTm DBS).

Six participants with msTBI who were between 3 and 18 years post-injury underwent surgery with electrode placement guided by imaging and subject-specific biophysical modeling to predict activation of the CL/DTTm tract. The primary efficacy measure was improvement in executive control indexed by processing speed on Part B of the Trail Making Test (TMT-B).

All six participants were safely implanted. Five participants completed the study and one was withdrawn for protocol non-compliance. Processing speed on TMT-B improved 15% to 52% from baseline, exceeding the 10% benchmark for improvement in all 5 cases.

CL/DTTm DBS can be safely applied, and may improve executive control, in patients with msTBI who are in the chronic phase of recovery.

Introduction

Moderate to severe traumatic brain injury (msTBI) often leads to enduring physical, cognitive, emotional, and behavioral impairments[1–7]. Cognitive dysfunction is the dominant

factor underlying persistent functional disability following msTBI[5,6,8] and correlates with both injury severity and performance on standardized neuropsychological assessments[9]. Characteristically, cognitive dysfunction in msTBI impacts executive control underlying task switching and organizing activities, sustained attention, information processing speed, and resistance to mental fatigue[5–8,10]. The msTBI population is estimated to number more than 5 million individuals in the US[11] who remain unable to return to prior levels of functioning within their communities[12]. At present, there is no effective therapy for the disabling effects of injury-related impairments in attention, executive function, working memory, or information processing speed. The sustained nature of cognitive impairment in msTBI contrasts with the more transient impairments seen in mild TBI[13], suggesting that the underlying pathophysiologic mechanisms of msTBI and mild TBI are distinct. The specific pathophysiology of msTBI suggests both a mechanism and a potential remediation strategy, and these considerations motivate this study.

Several lines of evidence indicate that the major persistent cognitive deficits in msTBI primarily reflect dysfunction of neurons within the frontal cortex and striatum[5,6,10,14–16], including a set of medial pre-frontal regions (particularly rostral anterior cingulate cortex, medial pre-frontal, and supplementary motor area) with strong functional interconnectivity. Cognitive impairment following msTBI is further linked with alteration of subcortical functional and structural connections of these frontal cortical regions with subcortical structures[15,17,18]. Atrophy of the left thalamus has been specifically correlated with executive dysfunction after msTBI[18].

A critical brain region linking these frontal cortical and striatal neurons into ‘fronto-striatal’ networks supporting executive functions is the central lateral (CL) nucleus of the thalamus[19–25]. CL neurons provide input to pre-frontal/frontal cortex and striatum[19–25] and optogenetic stimulation of CL activates these structures extensively in rodents[25]. Individual CL neurons broadly innervate the rostral striatum and frontal cortex[21]. CL projections to specific layers of the cortex support its unique role in enhancing activity of its cortical target regions[20,23]. Within the striatum, CL projections are particularly effective in driving action potentials from primary striatal output neurons[22] which in turn increases their inhibition of the globus pallidus pars interna, further releasing additional thalamic activation of the cortex (see Extended Figure 1). Collectively, these specializations likely enable recruitment of CL neurons by forebrain arousal regulation mechanisms during effortful mental activities which tax sustained attention, planning, decision-making, and working memory resources[19,20,26]. Underactivation of CL is proposed as a key factor in functional down-regulation of frontostriatal networks after brain injuries under the ‘mesocircuit hypothesis’[27] for functional recovery from impaired consciousness; incomplete recovery of neuronal function within these same networks is proposed to underlie persistent cognitive slowing and impaired executive function[27]. These observations suggest a practical therapeutic strategy for reversing the enduring cognitive deficits in msTBI: direct electrical stimulation of the remaining functional afferents emanating from CL via deep brain stimulation (DBS) (Extended Figure 1).

We sought to translate these insights into a practical strategy for human CL deep brain stimulation by performing a feasibility study (NCT02881151) to evaluate its safety and

efficacy in human subjects with chronic TBI-related disability impacting everyday function and employability. Informed by our prior studies in humans[28] and non-human primates[19,29], we chose the lateral portion ('wing') of the central lateral thalamic nucleus along with its associated fiber bundle, the dorsal tegmental tract, medial component (DTTm)[19,29,30] as the stimulation target (Supplementary Figure 1A–F). We developed biophysical models to guide virtual DBS electrodes within each subject's CL/DTTm to stimulate along the axis of the CL/DTTm fiber bundle based on location and stimulation amplitudes[31], and used the predicted activation models to evaluate and set criteria for successful CL/DTTm activation. The use of novel imaging and thalamic segmentation protocols, as well as predictive biophysical models estimating activation of projection fibers enabled very precise and accurate location of the CL nucleus and DTTm fiber bundle in individual human subjects. We then examined the safety and efficacy of this intervention for improving the persistent cognitive deficits of msTBI. As the primary efficacy endpoint, we selected Part B of the Trail Making Test (TMT-B), based on the well-established relationship between diffuse axonal injury (DAI) produced by msTBI and persistent dysfunction in attentional control and information processing speed[5,6,8,9,32].

Results

Patient disposition

Based on patient recruitment activities (see Supplemental Material) we received 419 inquiries for information about the trial. Candidates initially underwent telephone screening, which included administration of the Glasgow Outcome Scale-Extended (GOS-E) Structured Interview to ensure that the candidate had not returned to pre-injury level of vocational or educational function (GOS-E rating no higher than 5). From these initial inquires 15 individuals were consented for further assessment to confirm eligibility. Consent was obtained under a single IRB approved protocol at Stanford University. Of these, 9 candidates were excluded and 6 met all eligibility criteria and were enrolled and randomized between August 2018 and May 2021 (See CONSORT Diagram, Figure 1). The six adults enrolled all had a history of moderate to severe TBI (Glasgow Coma Scale score: 3–12) with persistent neuropsychological impairment and functional disability (Glasgow Outcome Scale - Extended score: 5–7)[33] (see Methods). We established baseline cognitive, psychological, and quality of life status (Table 1 Demographics). We sought to recruit participants representative of the general population of those with msTBI in terms of sex which is anticipated to yield a 2:1 Male:Female ratio; ultimately, we enrolled 4 men and 2 women based on self-report. We did not collect disaggregated sex and gender information.

Following CL/DTTm-DBS implantation, participants were randomly assigned to one of three post-surgical baseline conditions lasting 30, 44, or 58 days. The staggered baseline design was intended to identify acute CL/DTTm-DBS effects within individual participants and across participant pairs in response to initial stimulation exposure (short, intermediate or long baseline). Participants next entered a 14-day stimulation titration phase to identify optimal stimulation parameters. After completion of the titration phase, participants completed a 90-day open-label treatment phase during which they were exposed to CL/DTTm-DBS for 12 hours per day. Finally, participants were randomly assigned

to a 21-day treatment withdrawal or continuation condition to assess for loss of effect; this was double-blinded to minimize the influence of examiner and participant bias on final outcome assessment. The outcome assessment battery and electrophysiologic studies (described below) were repeated upon completion of the post-surgical washout, treatment and post-treatment withdrawal phases. The primary endpoint was the change in completion time on the TMT-B from pre-surgical baseline to the end of the 90-day treatment phase (see Supplemental Material for a discussion of study design considerations).

Primary endpoints

Part B of the Trail Making Test (TMT-B) served as the primary outcome measure. Performance on the TMT-B is thought to reflect executive control of attention, as working memory and set-switching capacity are challenged under speeded conditions[34]. We defined our primary endpoint as at least a 10% decrease (i.e., improvement) in completion time from presurgical baseline to the end of the treatment phase. Similarly, we defined decline as at least a 10% increase (i.e., worsening) in TMT-B completion time from presurgical baseline to the end of the treatment phase (see Methods).

Five of the six participants completed all four outcome assessments (the sixth participant exited the study prior to administration of the baseline assessment). All participants met the pre-selected primary endpoint (benchmark: 10% improvement from pre-surgical baseline to the end of the treatment phase; average improvement 31.75%; range 15% to 52%) (Figure 2A). While the two participants with the greatest initial deficits (P3 and P6 see Extended Table 1) experienced the most improvement (>40%), even those whose baseline performance was within the normal range (P4 and P5) improved by more than 20% (Extended Table 1). For the demographically-adjusted T-scores (mean= 50: SD= 10), the average improvement was 9.6 points (Extended Table 1), which represents a change of approximately one standard deviation of the population distribution[35].

Secondary endpoints

On the pre-selected secondary endpoint, change in TBIQoL-Fatigue, two participants met the improvement benchmark, two remained stable, and one met the benchmark for decline (Figure 2C). On the TBIQol-Executive Function subscale, four of the five participants that completed the trial exceeded the 10% improvement benchmark (mean= 32.7%, min= 0, max= 62%).

Figure 2C graphs the number of participants who exceeded the 10% improvement benchmark on each measure in the test battery. All five study participants also showed improved performance on the TMT-A, which assesses visual search speed[34] and may be linked to frontostriatal function and information processing speed (as discussed below).All 5 subjects also met the 10% improvement benchmark for the TBIQol-Attention subscale, (mean= 79.5%%, min= 50, max= 130%).

The Ruff 2&7 test, a measure of selective attention under speeded conditions, also showed broad improvements, (Figure 2C, Supplementary Table 2, and see Supplemental Methods) across the four participants who completed this test in full (P1’s data were invalidated due to test administration error). All four participants showed improved speed difference

greater than 10% (range 12% to 68% improvement in 'Total Speed', Supplementary Table 1), and three of the four showed improvements in controlled search speed (17% to 70% improvement, Supplementary Table 1) and auto detection speed (20% to 54% improvement, Supplementary Table 1. Additional behavioral results are shown in Supplementary Tables 2–6).

Two participants (P1 and P4) improved in global level of functioning from the lower moderate disability category of the Glasgow Outcome Scale-Extended (GOS-E) to the upper moderate disability category. These changes reflect recovery of work capacity (from inability to work to work at reduced capacity) and resumption of routine social activities with family and friends. Functional status remained stable in the other three participants (P3: lower moderate disability; P5 and P6: upper moderate disability) (see Supplementary Tables 2–6).

As part of the study plan, TMT-B performance was also measured at two intermediate time points (post-surgical, and treatment start), both of which followed some exposure to DBS. Since measurements at these timepoints likely were influenced by a wide range of other factors (e.g the surgery itself, time from surgery hours of stimulation exposure before measurement), they were not part of the pre-specified outcome assessment. For completeness, these results are shown in Extended Figure 8. Three of five subjects agreed to participate in a planned randomized blinded withdrawal phase (see Supplemental Material, and Supplementary Table 7). Only one subject randomized to the OFF condition (P3) and demonstrated a 34% decline in TMT-B score consistent with a withdrawal effect.

In addition, each participant and family members underwent semi-structured interviews as part of a parallel study (see Supplementary Table 8[36,37]).

Safety

Safe conduct of the study was monitored by a clinical oversight committee consisting of the 5 Principal Investigators (JMH, NDS, JTG, CRB, and AGM) and 2 independent medical monitors. The committee was convened at the beginning of the study and met quarterly to discuss study progress. All adverse events were reviewed with the committee and their adjudication agreed on following group discussion. Study continuation was predicated on a unanimous vote of the committee at each meeting.

All six participants underwent successful placement of bilateral DBS leads (Medtronic 3387) with no acute complications. There were 14 adverse events, two classified as serious (requiring hospitalization), see Supplementary Table 9. All adverse events resolved without sequelae. The majority of adverse events were mild and self-limited, consisting of typical postoperative symptoms. One participant developed a postoperative scalp infection requiring explantation of the system prior to the titration phase of the study. This participant was subsequently withdrawn from the study. One participant experienced back pain, neck pain, headache and hamstring tightness beginning several days after surgery, which were attributed to possible aseptic meningitis. These symptoms resolved over the course of one week. Another participant experienced difficulty with planning, organization and word

recall, which persisted over the course of approximately 2 months and was felt to be possibly due to stimulation.

Post-hoc analyses

Inter-subject consistency of electrode implantations within the human CL/DTTm—To translate pre-clinical findings that identified CL neurons[25], the 'lateral wing'[19,25], and the associated DTTm fiber bundle[19,29,30] as the primary structure for DBS activation, we developed a specialized data processing pipeline (see Supplemental Material and Supplementary Figure 1A–F). Figures 3A–F illustrate the approach to post-implant target localization and stimulation in a representative participant (P5). Panels A and D identify the location of active electrode contacts (L3 and L4 on the left side, R3 and R4 on the right side) displayed on coronal WMn images with CL boundaries shown in red. Panels C and F show CL/DTTm fiber bundle model activation achieved within the left and right hemisphere. Relative activation was estimated by calculating the percentage of fibers in each fiber tract that reached the threshold for activation[31]; these percentages were expressed using a histogram for each of four key fiber tracts for each lead position: CL/DTTm, MD, VPL and Cm (Figure 3, panels B and D for left and right sides, respectively). In this participant, combined stimulation of the four active contacts achieved a predicted 81% activation of CL/DTTm fibers within the left hemisphere and 78% activation of these fibers within the right hemisphere. The histograms plotted in panels B and E show the percentage of activation for CL/DTTm, MD, VPL, and Cm fibers with voltages between 1V and 5V applied to each of the four contacts. For most contacts CL/DTTm fiber activation dominated the range of current (or voltage, see Methods) amplitudes modeled for single contact monopolar activation. These histograms guided interpretations of findings obtained during titration testing used to establish selection of specific electrode contacts and stimulation parameters in the treatment trial (See Methods and Extended Figures 2–6).

Based on the activation profiles modeled for each participant (Figure 3 and Extended Figures 2–6), we sought electrode positions and orientations that were predicted to provide strong and selective activation of the target CL/DTTm fibers, compared to fibers associated with MD, VPL and Cm. The activation profiles predicted for the combination of active electrode contacts chosen for each participant by hemisphere are shown in Figure 3G. In all participants, selective and strong activation of left-hemisphere CL/DTTm fibers was predicted, though the degree of selectivity varied. Predicted activation of right-hemisphere CL/DTTm showed greater variability. In P4, our pre-surgical modeling did not predict activation of modeled right-hemisphere CL/DTTm fibers from the post-operative placement of this electrode (0.5% predicted activation) but as shown below (Figure 5) electrophysiological measurements demonstrate similar activation patterns of both hemispheres in P4; this discrepancy was hypothesized to reflect distortion effects of a small hemorrhage within the right thalamus on the DTI modeling leading to a drop out of modeled fibers (see Extended Figs. 4 and 5 and discussion below). Final stimulation parameters for each participant were chosen after a sequence of titration testing steps during which stimulation parameters adjusting the shape of the activation field (contact geometries, amplitudes of current or voltage, and pulse width of stimulation) were adjusted to maximize activation of modeled CL/DTTm, limit activation of modeled avoidance fibers, and to

strictly eliminate observed side effects during testing (Supplemental Material, Titration Phase). Across the participants final parameters ranged: 150–185Hz, 60–90us pulse width, 3.1–4.0V / 3mA, 3.3–5.1uC/cm2/phase).

To compare electrode placements across the five participants we developed a synthetic atlas to organize all participant electrode placements within a single common brain space (see Methods). Figures 4A–C illustrate the placements of active contacts for all participants in this common synthetic atlas space, demonstrating a tight clustering of active contacts for left hemisphere electrodes around the emergence of the CL/DTTm fibers exiting the CL nucleus boundary, with greater spatial variability for the active right hemisphere electrode contacts, particularly the lower active contact. This reduced placement precision on the right side was felt to be due to brain shifts induced by loss of cerebrospinal fluid during the procedures as the right hemisphere electrodes were placed after the left in four of five participants that completed the trial. Supplementary Videos 1 and 2 (rocking left right, showing pre-op versus post-op contacts, respectively) compare the pre-surgical and post-surgical placement clusters illustrating that left hemisphere post-surgical placements adhered closely to the initial plan with larger discrepancies between pre vs post placements on the right side. Supplementary Video 3 illustrates the entire surgical planning and outcome assessment process Figure 3G graphs the relative activation percentage for CL/DTTm and the avoidance fibers from MD, VPL, and Cm. For all participants, left hemisphere electrodes produced strong activation of the modeled CL/DTTm fibers; right hemisphere lower contacts showed greater variability.

To establish and evaluate consistency of physiological effects across participants we measured evoked responses in the electroencephalogram (EEG) to repetitive low-frequency stimulation (Methods). Figure 5 shows superimposed cortical evoked potential time tracings obtained across a 256 channel EEG array for activation across two therapeutic contacts (obtained before Treatment Phase. excepting P3, see Supplementary Table 11). Evoked potentials were driven by 100ms trains of stimulation (150–185Hz) on a 2Hz duty cycle of stimulation (see Supp. Table 12 for full stimulation parameters for each participant); stimulation bouts occur at 0–100ms on the displayed plots (gray shade; Figure 5A, C, see also Methods and Supplementary Results Figures 2–11). Across both hemispheres, evoked responses typically demonstrated an initial positive deflection peaking at ~200ms (vertical red lines, Figure 5). Topographical plots indicating the spatial variation in depth of evoked response at the time of the peak (~200ms) show that the strongest response appears within the frontal regions of the ipsilateral hemisphere between the medial and lateral regions (see Supplementary Figures 2–11 for channel-by-channel evoked response profiles). As seen in Figure 5, the left hemisphere showed more reproducible localization, depth of modulation and timing of peaked amplitude responses across all participants. Comparing these findings to those obtained from the synthetic atlas in Figure 4, this likely corresponds to the tighter clustering of the left vs right electrode contact placements (especially true for the bottom active contacts) across participants (see Extended Table 2), suggesting greater inter-subject consistency of activating the same fiber system in the left hemisphere. The clustering of the active contacts shown in panel E and F of Figure 5 demonstrates that the targeting methods used here (Figure 4, and Extended Figures 2–6) to identify the outflow of fibers from the lateral wing of CL into the DTTm are consistent across participants despite the wide variation in atrophy evident in this group (Extended Figure 7, Supplementary

Figures 12–17). As seen in Supplementary Video 2, the right sided lead placements showed greater variance in tip placement than at the top contacts used for activation in the trial. Of note, despite the lack of activation of CL/DTTm in the activation modeling for P4's right hemisphere, both of P4's hemispheres show evoked potentials of comparable time course and spatial localization in the frontal cortex. This indicates that P4 received therapeutic stimulation in both hemispheres.

Comparison of TMT-B performance results with two cohorts studied by Dikmen et al.—To estimate the likelihood that an average change in TMT-B completion time of this magnitude could occur spontaneously, we compared our results with those obtained from two subgroups of patients with msTBI who were followed by Dikmen et al.[5] at: 1) (n=146) 6 months post-injury and again 1 year post-injury (a test-retest interval comparable to the present study), and 2) (n= 118) who were followed 1 year post-injury and again between 3 to 5 years post-injury (a time since injury comparable to the present study). Test-retest improvement of the five participants in our study contrasts significantly with the natural history changes documented by Dikmen, et al. in both subgroups (Figure 2B). In our sample, TMT-B completion times improved 15 to 52% from pre-surgical baseline to treatment end. In comparison, test-retest changes in the 6 month to 1 year Dikmen et al.[5] sample were on average improved in TMT-B raw performance by < 4% (the difference between our study and this cohort is significant at $p<0.02$ [$p=0.011$](Kolmogorov-Smirnov test, K-S). For the 1 year to 3-to-5 year subgroup, the test-retest changes in the Dikmen et al.[5] sample were on average (geometric mean), 4% slower ($p<0.005$, K-S test [.0041]); see Supplemental Material for comparisons with TMT-A..

Discussion

We found that CL/DTTm DBS improved executive function as assayed by our primary outcome measure (TMT-B, which assesses attentional control), related performative tests (TMT-A, TMT-B minus TMT-A) and independent quality-of-life assessment instruments (TBIQol Attention and TBIQoL-Executive Function). Although variable across participants, we also observed improvements on the secondary outcome measures addressing fatigue, psychological health, and global level of function. None of the participants met the benchmark for decline on the primary outcome measure and only one participant (P5) did so on the secondary outcome measure.

One of the goals of this study was to develop a detailed surgical planning procedure for accurately targeting the CL thalamic nucleus at a specified angle of alignment designed to optimize stimulation of the fiber tract associated with CL (DTTm)[19,29,30]. To do this we innovated a pre-processing pipeline (Supplementary Figure 1) that included novel use of white-matter-nulled MRI, automated thalamic segmentation, diffusion tensor imaging and biophysical modeling of applied electric fields. While we cannot be certain that all these steps were necessary, we can say that the targeting strategy used in this work differs significantly from previous DBS targeting methods. Our findings shown in Supplementary Figures 12–17 demonstrate that despite the wide range of brain atrophy and hemispheric asymmetries across our participants, use of the pre-processing pipeline and positioning and alignment within CL/DTTm resulted in a tight clustering of active electrode contacts

within the synthetic atlas thalamus. These results support our interpretations below that the observed electrophysiological and behavioral effects reflect bi-hemispheric activation of the human CL/DTTm in the participants.

The pre-selected primary outcome measure, TMT-B, improved after three months of CL/DTTm DBS in all five participants who completed the trial (average 31.7% reduction in speed of performance). Of note, this finding was observed in persons with chronic disability (≥ 2 years post-injury) caused by moderate to severe TBI. Baseline performance on the TMT-B ranged from severely impaired to the upper limits of the normal range. These results thus comport with improvements in both performance accuracy and reaction times observed in intact non-human primates carrying out executive task during CL/DTTm DBS[19,29]. Several related measures capturing performative and qualitative aspects of improved executive attention also showed significant improvement, including TMT-A performance (average 30.7%), Trails B-A time (average 32%), TBI-QoL-Attention (average 79.5%), and TBI-QoL-Executive Function (average 32.7%). Despite the wide range of baseline scores noted on the TMT-B, performance improved by an average of approximately one standard deviation (~10 units of T-score) on both TMT-B and TMT-A, based on demographically-adjusted T-scores (Extended Table 1). The T-scores reflect population norms and this effect size is considered a clinically meaningful change[35]. These findings contrast with the large observational study of msTBI of Dikmen et al.[5].

To test the robustness of our conclusions, we compared our cohort to two cohorts in that study – one comparable in test-retest interval, and one comparable in duration since injury. We find that our effect sizes demonstrate significant improvement over that seen in both control groups (Figure 2B, Supplementary Figs. 18,19). Our sample also demonstrated complementary improvements in self-reported attentional (TBI-QoL-Attention) and executive (TBI-QoL-Executive) functions associated with real-world behavioral competencies and subjective ratings of quality of life[2–7,38]. These results are further supported by a parallel study involving these participants and their paired family members who underwent qualitative interviews and reported many real-world impacts enabled by these improvements (see Supplementary Table 8, cf. [36] and Fins et al. *in press*).

We interpret our findings of improved executive attention as the result of activating the CL/DTTm axonal projections (originating primarily from CL neuronal cell bodies) to partially deafferented neurons across Brodmann areas 6/8 (pre-motor, pre-SMA/SMA/FEF), 24 (anterior cingulate), 46 (dorsolateral prefrontal), and the rostral striatum. These regions have demonstrated monosynaptic connections with CL in rodents and non-human primates[39–41]. The centering of evoked fields between lateral and medial frontal cortical regions (Figure 5, Supplementary Figures 2–11) is consistent with these anatomical connections; however, we note that the evoked response profiles cannot resolve local cortical regional activations although future analyses with source localization methods might add further detail. Clinical and neuroimaging studies of msTBI subjects link their functional neuropsychological impairments, including impaired TMT-B performance, to initial deafferentation severity[5,7,9] and loss of corticostriatal connectivity[14–16]; specifically, loss of connections of medial frontal cortical regions including anterior cingulate cortex[14,15]pre-supplementary motor area (pre-SMA) and superior frontal gyrus[16] with the striatum. The pre-SMA and rostral

striatum are critical regions that facilitate decision-making under time-pressure[40] and are both heavily innervated by CL afferents[21,40]. A study of structural MRIs in 157 msTBI subjects[18] identified two key observations relevant to our findings: widespread brain atrophy is typical after only six months following msTBI and observed persistent impairment in executive function is associated only with atrophy of the thalamus in the dominant left hemisphere. Since we achieved greater consistency of placement of the electrode in the left hemisphere as shown in the synthetic atlas results (Figure 5) and more consistently localized cortical activations with activation of left hemisphere electrode contacts (Figure 5), our results may predominantly reflect compensation for left hemispheric dysfunction. Our participants, however, like the broader msTBI population[18] demonstrate bilateral atrophy and varying degrees of multi-focal cerebral injury (Supplementary Figures 12–17).

The primary effects of CL/DTTm stimulation as assessed by the TMT-B likely depend on activation of large myelinated axons within CL/DTTm *per se* perhaps with contribution from additional axons of cells within closely positioned paralaminar regions of the median dorsalis nucleus[42]. Cell bodies within the 'lateral wing' of CL[42] project to the rostral striatum and prefrontal/frontal cortical regions[39–42]. In intact non-human primates, stimulation of CL/DTTm facilitates executive attention in intact animals[19]; conversely, a loss of the behavioral facilitation produced with CL/DTTm stimulation occurs when stimulation combines activation of nearby Cm projections passing through the thalamic reticular nucleus into the DTTm bundle[29]. This experimental observation is also consistent with our findings that transient sensory and other side effects emerged in several participants when stimulating via the lower contacts, which were within or near Cm (see Supplemental Material). Recent experimental studies have also shown that stimulation of CL is selectively effective to emerge non-human primates from general anesthesia using both microstimulation methods[20] and macrostimulation methods that activate both CL and MD[43,44]. Importantly, VA/VL stimulation is experimentally non-effective supporting our interpretation here that observed effects of upper contacts placed just outside the nuclear boundary of CL produce activation of CL/DTTm *per se*. Consistency of activation of DTTm fibers by the upper contacts (as shown in Figures 3G and 4) supports the role of these contacts in further activation of CL outflow as opposed to local neuronal populations in VA/VL *per se*.

Neocortical neurons markedly change their firing patterns following even small increases in membrane potential depolarization[45]. We propose that CL/DTTm DBS effectively increases the depolarization tone of frontostriatal neuronal membrane potentials across these cortical and subcortical populations, and that these changes in membrane potential underlie the behavioral improvements observed here. As shown in Supplementary Figures 12–17, all of our subjects had dilatation of their ventricular systems along with cortical and subcortical atrophy, suggesting broad bi-hemispheric deafferentation of frontal and striatal neuronal populations. The partial deafferentation of these neurons resulting from msTBI can be expected to associate with reduced depolarization tone and lower average resting membrane potentials than those observed in the intact brain[45]. The resulting increase in excitatory synaptic activity on monosynaptically connected neocortical and striatal neurons induced by CL/DTTm DBS (~150Hz pulses for 12 hours daily) likely increases membrane depolarization in these cells (cf. [46]).

The marked shift in level of tonic input to neocortical neurons produced by CL/DTTm DBS may have a variety of effects: it may improve spatiotemporal integration within cortical pyramidal neurons, which is strongly influenced by overall background synaptic firing rates[47]; it may trigger specific high-frequency thresholds for synaptic activity that in turn control a variety of mechanisms of dendritic electrogenesis in neocortical Layers II, III, and V[48,49]; it may act at the network level as a high frequency noise input to improve coincidence detection (cf. [48]); and it may restore the dynamic range of neocortical neurons via gain control mechanisms that depend on synaptic background activity[50,51]. Thus, restoration of depolarization tone is collectively expected to induce mechanisms that normalize integrative activity within frontal cortical and striatal neurons and, consequently, at the network level. In support of this notion, studies in intact non-human primates demonstrate that CL/DTTm DBS produces changes at the network level by increasing the depth of task-related modulations of neuronal activity in frontostriatal neurons[52].

Importantly, this mechanism can be directly tested in human subjects in future studies: longitudinal increases of neuronal GABAergic tone (a physiological index of intraneuronal inhibitory tone) within frontostriatal neuronal populations in msTBI subjects correlate with executive function providing support for the mechanism proposed here[53]. Increasing arousal regulation within wakeful states is primarily associated with increasing inhibitory tone within cortical neurons[46]; CL/DTTm DBS induced reversal of a selectively down-regulated GABAergic signal across these structures in association with TMT improvements is a sharp prediction of our results.

Our study has several limitations. The main limitation is that, while the effect size on the primary outcome measure, TMT-B, is large (in that we find TMT-B improvements exceed those observed in a comparable natural recovery cohort at timepoints after six months), the number of participants is small. The study is also underpowered to address many important questions that depend on between-subjects comparisons, including how observed effects on performative tests may interact with lesion site and mechanism, and how changes in self-report measures may reflect unmeasured psychosocial and economic factors. Additionally, our small sample does not allow assessment of how variations in treatment (precise electrode position and orientation in each hemisphere relative to the CL/DTTm target and target avoidance fibers) impact efficacy. Additional limitations include the incompleteness and variability of the planned blinded withdrawal phase, and the short timeframe of the study. The three-month treatment phase limits any systematic evaluation of long-term changes, management, and psychosocial impacts of the invention. A direct test of generalizability of our findings will require a randomized clinical trial with a large number of subjects studied with the same precision of targeting methods and verification of relative isolation of stimulation of the CL/DTTm. Another important limitation is the choice of TMT-B as the sole outcome measure to capture impaired executive attention and related aspects of executive function; future work should develop composite measures to broaden the range of effects tested (cf. [18]).

Methods

Participant recruitment

Participants were recruited through a variety of channels, including self-referral and provision of IRB-approved recruitment materials to academic research partners and consumer advocacy organizations serving patients with TBI. Recruitment materials identified the ClinicalTrial.gov number for the trial: NCT02881151. To accelerate enrollment, we also received IRB approval to subcontract with PatientWing (Philadelphia, PA), a digital media marketing firm specializing in clinical trial recruitment. PatientWing identified potential study candidates using key-word searches on several online platforms including Google and various social media channels. To ensure equal access to our trial, PatientWing also launched a print campaign during the heavy holiday travel season in several Greyhound bus stations throughout California, targeting individuals without access to the internet.

Examiner training, certification and oversight procedures

Call center personnel from PatientWing were trained by key study staff (Drs. Giacino and Kolakowsky-Hayner, licensed neuropsychologists) to conduct the telephone-based screening interviews. In addition, the neuropsychology staff conducted specialized training with five CITI and HIPAA-certified research coordinators who were responsible for administration and scoring of the CT-DBS Multi-Dimensional Outcome Assessment Battery (see below). Training was conducted remotely using webinars and Zoom-based demonstrations. Examiners also completed the on-line training protocol required for administration, scoring and interpretation of the Columbia Suicide Severity Rating Scale (C-SSRS). Following certification, all examiners received weekly virtual supervision by the licensed neuropsychologists. Separately scheduled troubleshooting meetings were held with research coordinators to address non-routine subject-specific issues and scoring ambiguities that arose in the context of test administration. GOS-E ratings were reviewed by key staff during team teleconferences to ensure accurate scoring and resolve ambiguities, which are commonly encountered on this measure.

Data quality assurance activities

Following development of the Case Report Forms, we constructed a REDCap database comprised of 196 data elements. We created automated error check functions which were monitored on an ongoing basis. Data were checked for missingness, errors, and out of range or invalid values.

Ethical considerations and consent mechanisms

The research was carried out under a single IRB approved protocol at Stanford University and participants gave written informed consent, according to CARE guidelines and in compliance with the Declaration of Helsinki principles. See Supplemental Material for additional discussion.

Study design

Eligibility criteria

Inclusion criteria: 1. History of moderate to severe TBI based on estimated GCS score within first 48 hours of injury (acceptable GCS range = 3–12); 2. Age 22–60; 3. At least 24 months from date of onset; 4. Fluent in English and able to independently provide consent; 5. Rating of lower moderate disability to lower good recovery on the Glasgow Outcome Scale-Extended (GOSE) at time of enrollment (acceptable GOSE range 5–7); 6. Failure to return to pre-injury level of vocational or educational function.

The above criteria differed from those defined at the onset of the trial, which were: Age 55 maximum, GCS 9, GOSE 6–7, and another criterion requiring a performance ≥ 2 SD's below the demographically-corrected mean on at least one attention, memory or executive function measure at baseline. All changes were approved by FDA amendment during the course of trial.

Exclusion criteria: 1. History of major developmental, neurologic, psychiatric or substance use disorder with evidence of disability prior to onset of TBI; 2. Lesions involving two or more of the following regions- orbitofrontal, ventral prefrontal, mesial temporal and thalamus; 3. Major medical co-morbidities that, in the judgment of the PI, significantly increase risk or significantly reduce the likelihood of benefit from DBS; 4. Malignancy with < 5 years life expectancy; 5. Untreated / uncontrolled (severe at the time of enrollment) depression or other psychiatric disorder; 6. Women of childbearing age who do not regularly use an accepted contraceptive method. Subjects who become pregnant after enrollment may be excluded from the study. Those who become pregnant prior to the surgical implantation of the DBS system will be excluded from the study; 7. Inability to stop Coumadin or platelet anti-aggregation therapy before, during and after surgery; 8. Previous DBS or other brain implants; 9. Previous ablative intracranial surgery; 10. Implantable hardware not compatible with MRI; 11. Hardware, lesions or other factors limiting placement of electrodes in optimal target location in the judgment of the operating surgeon; 12. Concurrent enrollment in any other clinical trial; 13. Any condition that, in the judgment of the PI, significantly increases risk or significantly reduces the likelihood of benefit from DBS.

Detailed clinical study design—See Supplementary Table 10 for detailed description of study phases.

Statistical design—Descriptive statistics (e.g., mean, median, percentage of change in raw and t-scores between timepoints) were calculated to summarize relevant participant characteristics. Both raw and t-score differences for behavioral measures were evaluated against a >10% cut-off that denoted improvement in each characteristic. SAS version 9.4 (SAS Institute, Inc., Cary, NC) was used for all analyses.

Target localization

Image acquisition: In addition to a conventional scan protocol used for clinical pre-surgical DBS planning, participants were scanned with a WMn-MPRAGE protocol (WMn) protocol

and a diffusion tensor imaging (DTI) protocol, on a 3T GE MR750 scanner using a 32-channel head coil.

WMn image volumes were acquired using the following parameters: 3D MPRAGE sequence, coronal orientation, TE 4.7ms, TR 11.1ms, TI 500ms, TS 5000ms, views per segment 240, FA: 8°, RBW +/−11.9kHz, spatial resolution 1mm isotropic, 220 slices per volume k-space ordering; 2D radial fanbeam, ARC parallel imaging acceleration: 1.5×1.5, scan time 8 min.

DTI image volumes were acquired using the following parameters: 2D diffusion-weighted single-shot spin-echo echo planar imaging (EPI) sequence, axial orientation, TE 74ms, TR 8000ms, RBW +/−250kHz, diffusion directions: 60, diffusion weighting (b-value): 2500 s/mm^2, spatial resolution 2mm isotropic, 70 slices per volume, parallel imaging acceleration: 2, scan time 11min.

WMnMPRAGE and DTI image volumes were visually inspected to ensure that scans were of sufficient quality for analysis and were not corrupted by motion artifact.

Segmentation: Whole-brain WMn volumes were processed with the THOMAS thalamic segmentation tool with no preprocessing. The THOMAS algorithm applied to WMn images has been validated against manual segmentation[62]. Using version v0 of this tool (https://github.com/sujason/thomas), we segmented and extracted the volumes of 12 lateralized structures in each hemisphere of the brain: whole thalamus, ten thalamic nuclei (anteroventral [AV], centromedian [Cm], lateral geniculate nucleus [LGN], mediodorsal [MD], medial geniculate nucleus [MGN], pulvinar [Pul], ventral anterior [VA], ventral lateral anterior [VLA], ventral lateral posterior [VLP], and ventral posterolateral [VPL]), and one adjacent epithalamic structure, the habenula (Hb). Note that THOMAS segments the whole thalamus separately from the thalamic nuclei; this whole thalamus encompasses all these preceding structures, as well as the mammillothalamic tract and some additional unlabeled thalamic areas (i.e., between segmented thalamic nuclei). In addition to THOMAS segmentation, we segmented the CL and VPM nuclei in each hemisphere using a single-atlas segmentation approach. This utilized manually-segmented CL and VPM nuclei, performed by a single expert neuroradiologist (TT) on the THOMAS template, which is an extremely high quality WMn brain volume formed by carefully registering and averaging 20 WMn volumes[62]. The CL and VPM single-atlases obtained this way were non-linearly warped to the WMn volumes of individual participants, and CL and VPM boundaries were finalized by trimming away any CL and VPM voxels which overlapped with THOMAS nuclei. In other words, THOMAS segmentations were allocated higher priority than CL and VPM segmentations – the rationale for this being that the THOMAS segmentations (obtained with a multi-atlas approach) were more accurate than the CL and VPM single-atlas segmentations.

DTI modeling: We used biophysical models to predict the degree of activation of fiber pathways seeded from several thalamic nuclei. Each pathway was created using deterministic tractography seeded from the following nuclei: Cm, CL, MD, VPL, VPM using DSI Studio (https://dsi-studio.labsolver.org/). Predictive models were created in

SCIRun (https://sci.utah.edu/software/scirun.html) and used to predict the percent activation of each pathway via stimulation at each electrode across a range of amplitudes from −1 to −5 V. The results of these simulations were summarized in activation histograms that provided a visual summary of hundreds of individual simulations and allowed comparison of relative activation of pathways for targeting or avoidance.

Surgical planning for DBS electrode placement: We developed a novel strategy for targeting the CL nucleus together with the fiber bundle of axons emanating from this region (medial portion of the dorsal tegmental tract, or DTTm)[30]. Based on known monosynaptic connections determined in prior physiological and anatomical studies we sought to stimulate cell bodies and axonal regions with reciprocal connections to the 'lateral wing' of CL[30] and prefrontal/frontal cortical regions including anterior cingulate (area 24)[39], premotor, pre-supplementary motor/supplementary motor area (area 6)[40], and dorsomedial prefrontal cortex including frontal eye fields (areas 8)[41]. In addition, we planned the DBS lead target and trajectory to stimulate fibers emanating from the paralaminar region of medial dorsalis nucleus (plMD) which have strong projections to dorsal lateral prefrontal cortex (area 46)[63]. Collectively, the primary monosynaptic projections in the expected stimulation regions span the medial prefrontal/frontal regions with some extension over the lateral convexity of the frontal cortex.

To guide electrode placements to achieve this targeting of CL/DTTm we employed a three-step algorithm that involved a group consensus judgement at each step in the process to evaluate quality of evidence and model fidelity. Initial targets / trajectories were determined with relationship to 1) automated segmentations of thalamic sub-nuclei using THOMAS augmented by the CL/VPM single-atlas approach; 2) modeling of dorsal tegmental tract medial (DTTm) fibers emanating from each patient's individual CL shell volume using the DTI data subject to tractography using DSI Studio; and 3) biophysical modeling of fiber activation using model electrodes placed in participant brain space. Electrode placements were adjusted for safety and angle of entry point, consideration of local blood vessel anatomy, and the maximal activation of the CL/DTTm fiber tract with minimal activation of off-target fibers (Figure 3, Extended Figures 2–6).

Prior to selection of a final surgical trajectory for each patient's electrodes, patient-specific imaging, fiber tractography, segmented thalamic nucleus targets and bioelectric field models were incorporated into a planning simulation. This simulation facilitated optimization of each subject's lead trajectories based on 3D-segmented anatomical targets and regions of avoidance, as well as finite element model (FEM) simulations predicting the outcome of a range of potential stimulation parameters. Team review of each separate stage of this algorithm resulted in selection of THOMAS model, DTI model and final chosen electrode positioning for pre-surgical planning.

The planning process, including lead positioning and bioelectric simulations, was performed using the open-source software project SCIRun. This software allowed MR and CT imaging to be combined with patient-specific 3D models of thalamic nuclei created using the THOMAS segmentation algorithm. Lead placement models produced in SCIRun also included fiber tractography generated using the THOMAS nuclei as seed regions, which

could be recolored following FEM simulations to represent fiber bundle activation in response to variable stimulation settings. A 3D representation of the Medtronic 3387 DBS lead was placed into each simulation and manipulated relative to AC-PC coordinates, allowing analogous trajectories to be explored both in Medtronic's StealthStation Surgical Navigation System and within the SCIRun model.

DBS lead placement was determined by a confluence of surgical safety considerations, investigated via the Stealth system, with anatomical targeting cues visualized within SCIRun. Special attention was given to placement of the electrode tip within the "lateral wing" of the central-lateral (CL) thalamic nucleus. This "lateral wing" was identified as the posterior projection of CL containing a bulk of its cellular somata as well as a majority of the efferent fiber tracts passing through the nucleus. To maximize activation of our targeted regions while avoiding activation of untargeted fibers, such as those projecting from Cm and VPL/VPM, electrodes were typically placed with their more proximal contacts outside of the body of CL, along the path of its projecting fibers (particularly those emerging from CL's lateral wing). This allowed for activation of CL-originating fiber tracts without requiring all active contacts to be embedded in the CL nucleus itself. Optimal lead placement required consideration of all the aforementioned elements within the SCIRun model, including the locations of cellular somata in each of the segmented thalamic nuclei as well as the shapes and projections of modeled fiber tracts.

Predicted activation of fiber tracts: Anatomical references (anterior and posterior commissures) and participant imaging assembled in SCIRun software were used to perform finite element model (FEM) simulations for each subject. FEM simulations provided insight for optimal surgical targeting as well as postoperative stimulation titration, with FEM-predicted activation serving as an initial guide for therapeutic stimulation parameter selection. These models were constructed using a simple activation function (AF), calculated from the second derivative of stimulation voltage. Fiber tracts were "activated" when AF values within the fiber crossed a threshold, providing a percentage estimate of activation within the fiber bundle. Activated fibers can be "painted" within the SCIRun model to provide a spatial representation of stimulation, for the purpose of comparing alternative lead positions and stimulation settings. The results of these simulations were also used to produce activation histograms, depicting the percentage of activation within five designated fiber bundles of interest.

Outlines of ideal DBS lead locations and thalamic nuclei of interest were embedded in MRI volumes by setting those regions' voxels to maximum intensity, then exporting in DICOM format. These volumes were loaded into the surgical planning software (Stealth FrameLink, Medtronic) to facilitate final planning of lead trajectories.

Surgical targeting and implantation—Participants were admitted for 1–3 days following the surgical procedure and discharged when stable and ambulatory, see Supplemental Material for detailed surgical methods.

Post-operative programming—A post-operative CT with 0.5 mm^3 voxels was acquired approximately 30 days after surgery. The purpose of this CT was to determine actual DBS

lead positions after any post-surgical pneumocephalus or brain shift had resolved. This post-operative image volume was co-registered with the pre-operative MRI volumes using ANTS. DBS lead positions were determined by aligning the electrode contacts with the lead artifact in SCIRun. At this point the virtual monopolar review was repeated to assess activation of fiber pathways at a range of amplitudes. New histograms were generated and were used to guide the cathode survey during participant programming.

DBS electrode contact evoked potentials—Electroencephalographic (EEG) responses to DBS were recorded prior to the treatment phase in four out of five participants, with one participant (P3) needing to postpone recording until after the treatment phase due to COVID-related restrictions in place during the pre-treatment timepoint. A high density 256 channel EEG array (Electrical Geodesics, Inc.) was placed on the scalp and NetStation Acquisition software (Electrical Geodesics, Inc.) was used to record DBS-evoked potentials at a sampling rate of 1000Hz. DBS was delivered by the implanted neurostimulator and consisted of 3 minutes of 100-millisecond trains of square-wave pulses (60μs or 90μs per phase) with an inter-train interval of 2 seconds, delivered in a bipolar configuration across two contacts of the same lead. The amplitude and frequency of the stimulation trains were patient-specific (Supplementary Table 11). Recordings were obtained for every adjacent bipolar contact configuration for the left (E0+/E1-, E0-/E1+, E1+/E2-, E1-/E2+, E2+/E3-, E2-/E3+) and right (E8+/E9-, E8-/E9+, E9+/E10-, E9-/E10+, E10+/E11-, E10-/E11+) hemisphere leads.

Evoked potentials were identified by manually marking the starts of stimulation trains in the raw data using NetStation Review (Electrical Geodesics, Inc.). This was done by a single investigator to eliminate interrater variability and checked by another investigator for accuracy. 80–94 evoked potentials that were free of muscle artifact were marked per bipolar contact configuration. Marked data were converted from the raw mff file format to the set file format accessible by EEGLAB v2021.1 software (https://sccn.ucsd.edu/eeglab/index.php) run on MATLAB R2021a (The Mathworks, Inc.). Briefly, the data were processed in EEGLAB as follows. Data were downsampled from 1000Hz to 250Hz and filtered with a 1Hz high pass filter. Line noise was then removed by the cleanLineNoise function of the EEG-Clean-Tools toolbox (PREP pipeline) v0.56.0 (http://vislab.github.io/EEG-Clean-Tools)[64] and re-referenced to the average signal. EEG contacts with excessive artifacts were identified and their data removed (number of removed channels reported in Supp. Table 13) and replaced by spherical interpolation by the clean rawdata and pop_interp functions of EEGLAB. Data were re-referenced again to the average signal. A final cleaning step was done with independent component analysis. Independent components were identified using AMICA v1.5 (https://sccn.ucsd.edu/~jason/amica_web.html) and labeled as brain signal, muscle artifact, eye movement, heart artifact, line noise, channel noise, or other using ICLabel v1.3 (https://github.com/sccn/ICLabel). Muscle artifact, eye movement, and channel noise components that were present at or greater than 50% in the data of EEG channels were removed (number of removed independent components reported in Supp. Table 13). Artifacts from blinks, cardiac activity, and muscle contractions were removed by rejecting the corresponding sources from an independent component analysis (ICA)

decomposition using the Infomax algorithm[65]. Data then underwent a final re-reference to the average signal.

Cleaned data were epoched from −100ms to 500ms, where 0ms is the start of the 100ms stimulation train, and averaged to create a mean epoch for each bipolar contact configuration. Mean epochs from reverse polarity bipolar contact configurations (e.g., E0+/E1- and E0-/E1+) were averaged together, creating a mean evoked potential map for each pair of adjacent contacts on a lead. This step was done to reduce the stimulation artifact and isolate the evoked potential[66]. Mean bipolar evoked potential maps were plotted to examine the latencies and scalp locations of the evoked potentials (Supplementary Figs. 2–11).

Supplementary Figures 2–11 show the DBS-evoked potentials obtained for the therapeutic contacts selected during the titration phase for treatment DBS for each subject. Overall, we observed robust evoked potentials localized to the ipsilateral frontal cortex, with the peak amplitude typically localized medially in the frontal cortex. This is consistent with animal anatomical literature showing CL's strong connectivity to the dorsomedial frontal cortex. Evoked potentials in the left hemisphere were more robust than those in the right hemisphere. This is likely due to the implantation of the left electrode first and the right electrode second, which reduced the effect of brain shift on targeting. In general, across-patient plots showed an initial rapid low amplitude potential (~0–20ms) likely corresponding to volume conduction of the DBS. This initial rapid low amplitude potential, with equally rapid decay, was localized to the ipsilateral side centered over the therapeutic contacts with the isolines demonstrating concentrated signal over the posteromedial frontal and anteromedial parietal cortices. The scalp electrode patterning for the initial potential was conserved across all patients.

Data availability

A minimum dataset extracted from the REDCAP database has been made available on Dryad: https://datadryad.org/stash/share/qJ1U_HqZYVgzadpn9vxF2CE6hhvGEQYHjARtQ3zs6uU

Extended Data

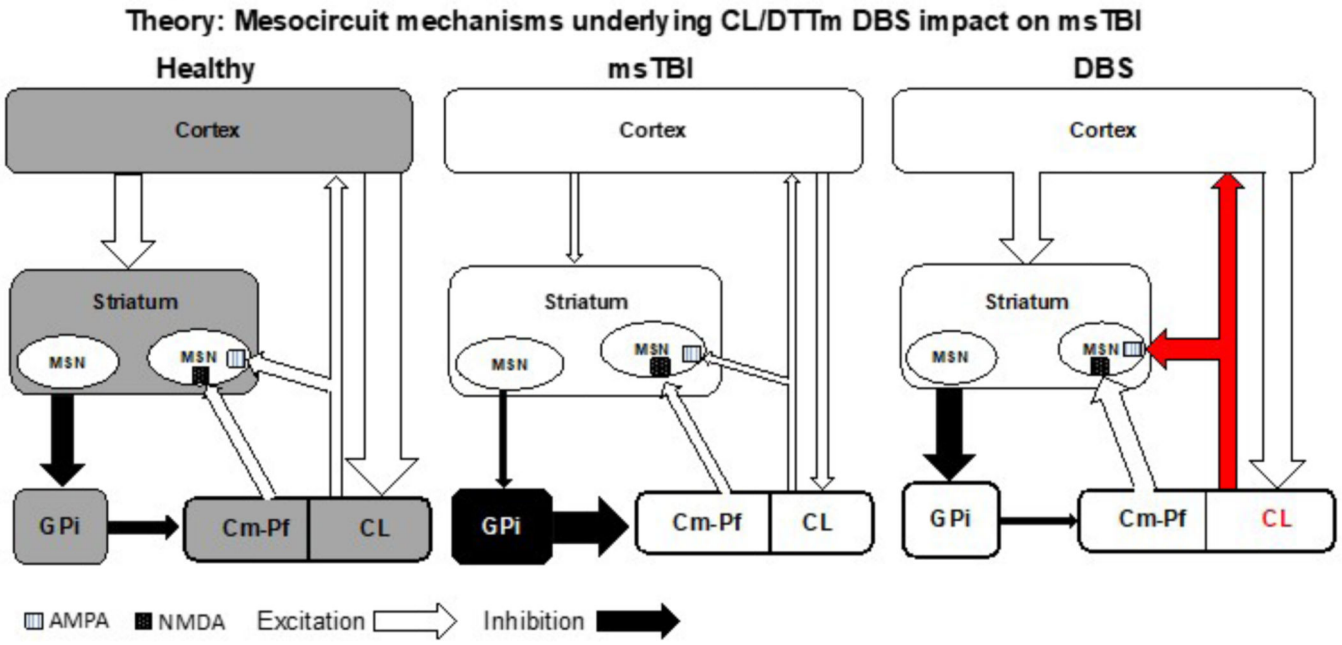

Extended Figure 1. Mesocircuit theory for recovery of anterior forebrain function with CL/DTTm DBS in msTBI.

Schematic diagram illustrating mesocircuit model for alteration of function following coma and moderate to severe brain injury and restoration of function with CL/DTTm DBS[27,54].

Left figure element: Healthy normative function of corticothalamic system. Projections of central lateral thalamic neurons to anterior forebrain mesocircuit and posterior medial complex[27,54]. CL co-activates frontal-parietal cortico-cortical connections and modulates their feed-forward and feedback connectivity via layer-specific effects within cortical columns[20,54–56]. CL specifically targets supragranular and infragranular cortical layers avoiding projections into the input layers[23]; these anatomical specializations support a proposed selective role in modulation of long-range corticocortical functional connectivity[56]. CL projections to the striatum strongly activate this structure via projections to medium spiny neurons, MSNs and act via AMPA receptors, whereas Cm-Pf afferents act via NMDA receptors[22].

Middle figure element: msTBI produces widespread deafferentation of the corticothalamic system leading to loss of CL modulation of cortex and striatum[27,54]. Two major consequences of this down-regulation of CL output in combination with overall reduction of cerebral background activity are: 1) marked reduction in corticothalamic and corticostriatal outflow, 2) shut down of the medium spiny neuron output from striatum to globus pallidum interna (GPi) producing increased thalamic inhibition and further reduction of thalamocortical and thalamostriatal outflow. Collectively, these changes are proposed to exert a disproportionate impact on the anterior forebrain[27,54].

Right figure element: CL/DTTm DBS is proposed to reverse the mesocircuit level effects of reduced corticothalamic, corticostriatal, and striato-pallidal output by direct overdrive pacing of CL output via the DTTm. This model for the effects of direct electrical stimulation

of CL/DTTm in msTBI is supported by animal studies that demonstrate broad activation of the frontal cortex and striatum with CL electrical stimulation[19,24,25]. These and related studies further show that CL electrical stimulation modulates executive attention and arousal in intact[24,25,57] and brain-injured rodents[58], intact non-human primates[19,29,52,59–61], and a human subject in the minimally conscious state[28]. Cortical evoked responses overlapping those observed here have been obtained in a human subject with CL DBS supporting the further generalizability of the findings[28].

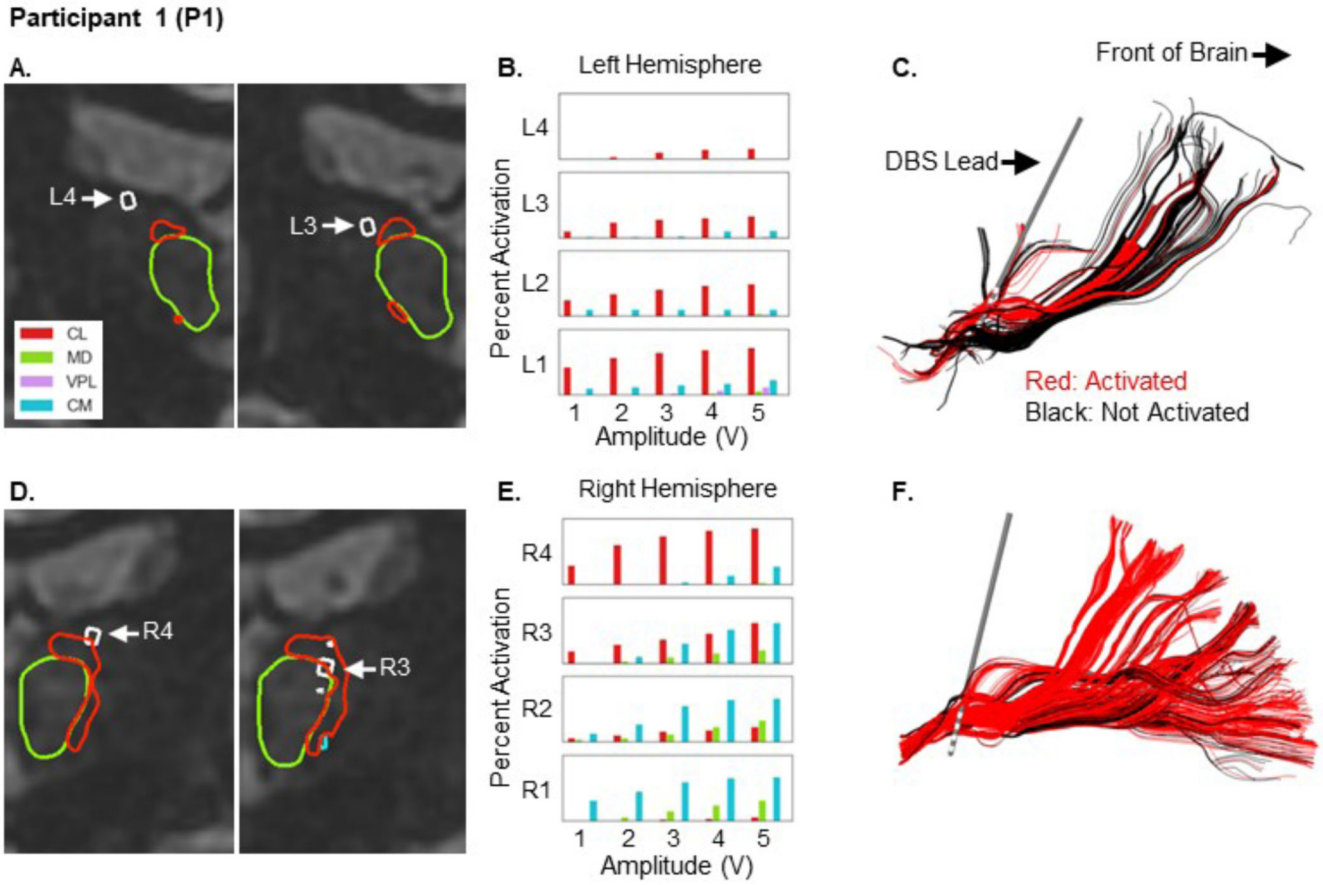

Extended Figure 2. Placement of DBS electrodes within the CL/DTTm target for subject participant P1.

A. Active contact locations and fiber bundles for left hemisphere of P1 rendered within P1 space, CL nucleus (red), MD (green), VPL (purple) Cm (cyan);

B. Histograms of fiber activation for left sided CL. MD, VPL, and Cm

C. DBS activation of fibers (red), inactive fibers rendered in blue.

D. Active contact locations and fiber bundles for right hemisphere of P1 rendered within P1 space, CL nucleus (red), MD (green), VPL (purple) Cm (cyan).

E. Histograms of fiber activation for right sided CL. MD, VPL, and Cm

F. DBS activation of fibers (red), inactive fibers rendered in blue.

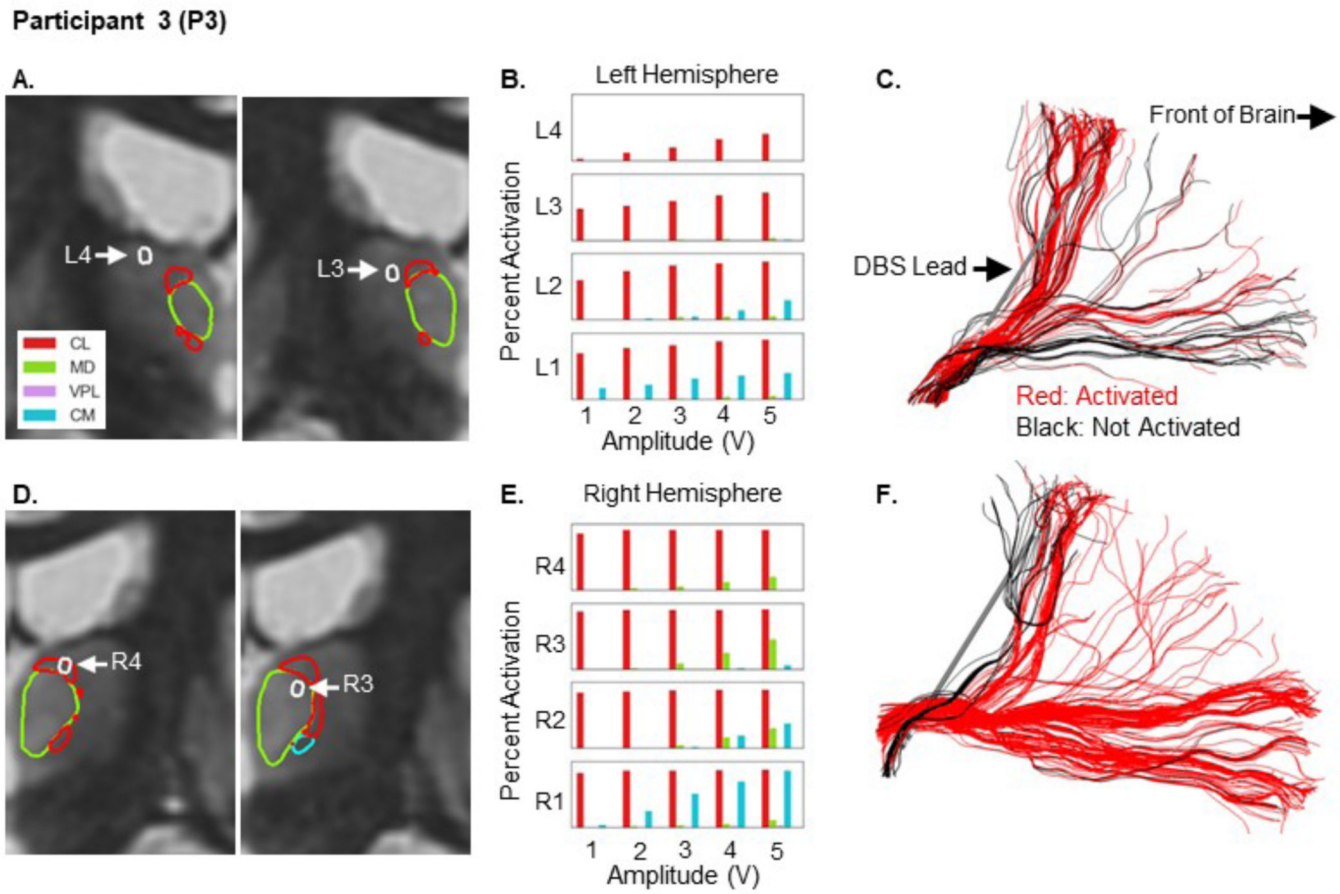

Extended Figure 3. Placement of DBS electrodes within the CL/DTTm target for P3.

A. Active contact locations and fiber bundles for left hemisphere of P3 rendered within P3 space, CL nucleus (red), MD (green), VPL (purple) Cm (cyan).

B. Histograms of fiber activation for left sided CL. MD, VPL, and Cm.

C. DBS activation of fibers (red), inactive fibers rendered in blue.

D. Active contact locations and fiber bundles for right hemisphere of P3 rendered within P3 space, CL nucleus (red), MD (green), VPL (purple) Cm (cyan).

E. Histograms of fiber activation for right sided CL. MD, VPL, and Cm.

F. DBS activation of fibers (red), inactive fibers rendered in blue.

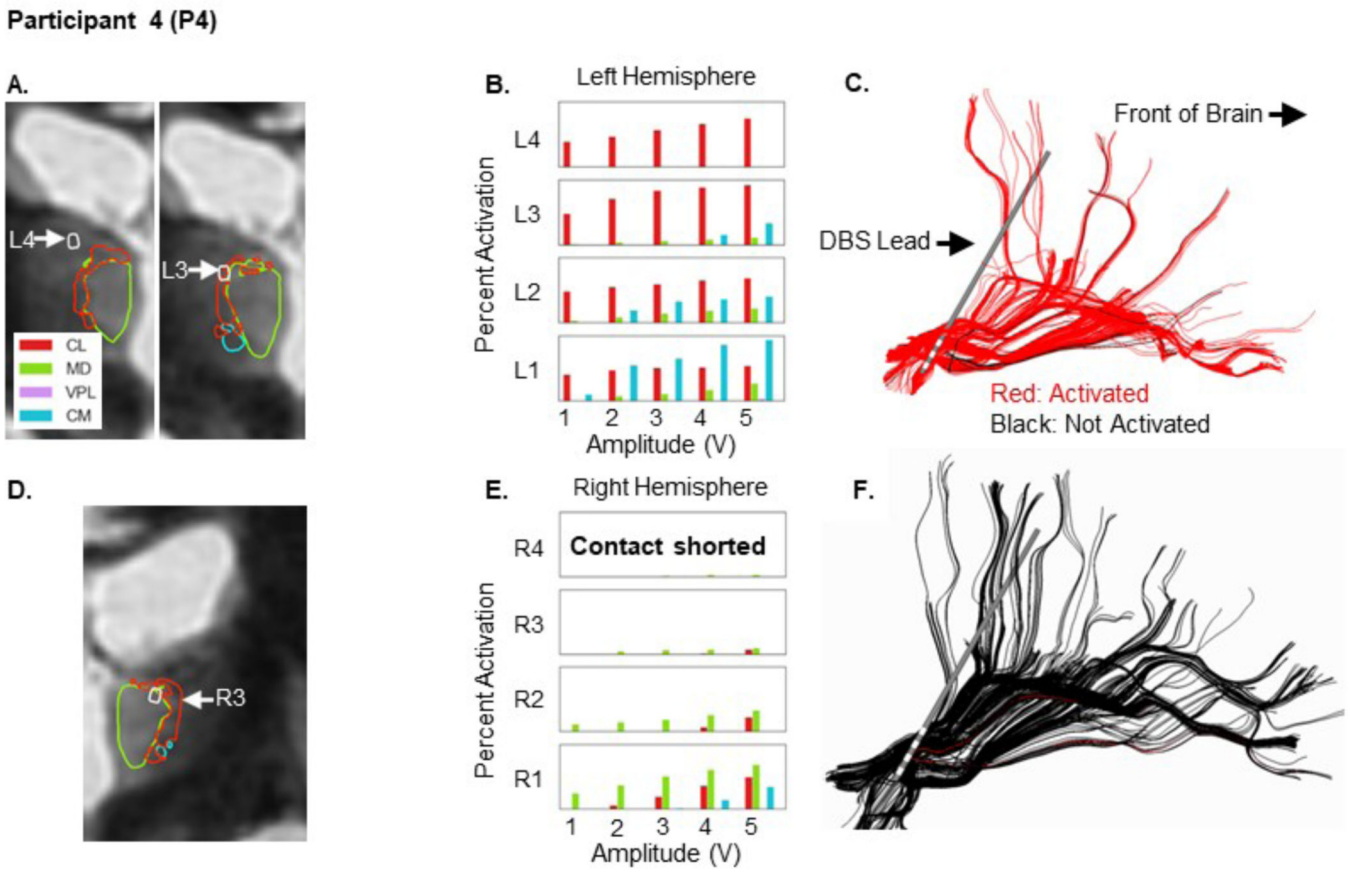

Extended Figure 4. Placement of DBS electrodes within the CL/DTTm target for P4.

A. Active contact locations and fiber bundles for left hemisphere of P4 rendered within P4 space, CL nucleus (red), MD (green), VPL (purple) Cm (cyan).

B. Histograms of fiber activation for left sided CL. MD, VPL, and Cm.

C. DBS activation of fibers (red), inactive fibers rendered in blue.

D. Active contact locations and fiber bundles for right hemisphere of P4 rendered within P4 space, CL nucleus (red), MD (green), VPL (purple) CM (cyan).

E. Histograms of fiber activation for right sided CL. MD, VPL, and Cm.

F. DBS activation of fibers (red), inactive fibers rendered in blue.

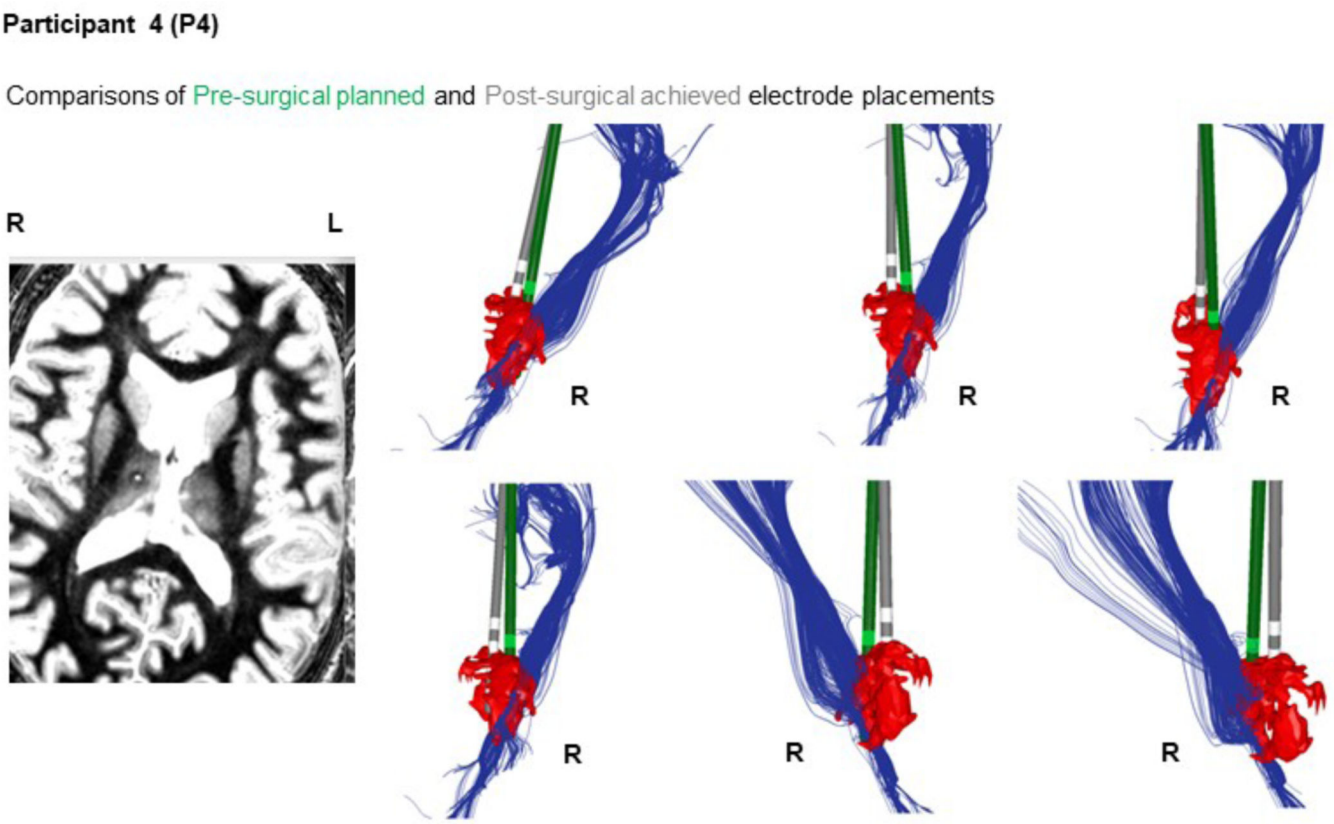

Extended Figure 5. Alteration of DTI model of CL/DTTm in P4 by local hemorrhage within right thalamus.

MRI image shows large susceptibility artifact in the right central thalamus secondary to duret hemorrhage. Right panels: Distortion of MRI signal in this region limits the formation of DTI modeled fibers as seen in the six views comparing the pre-surgical locations of electrode placements (green electrode models) and post-surgical actual locations (grey electrodes). As seen in each panel, post-surgical electrode placement is medial to planned location. As shown in Figure 5, a relative symmetry of cortical response is nonetheless obtained suggesting that more medial fibers associated with this pattern activation did not appear in the DTI model due to the loss of local signal in the region of the hemorrhage.

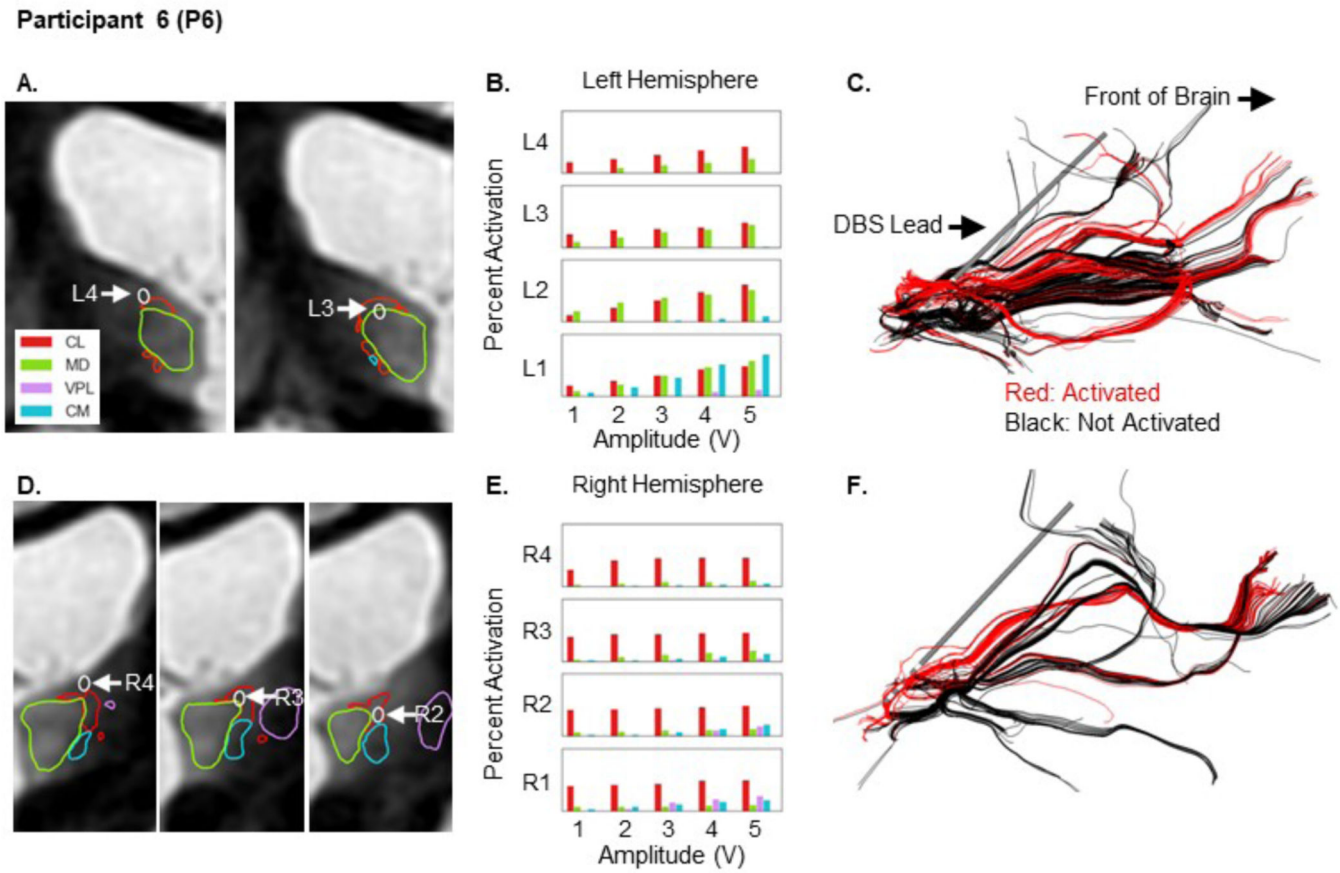

Extended Figure 6. Placement of DBS electrodes within the CL/DTTm target for P6.

A. Active contact locations and fiber bundles for left hemisphere of P6 rendered within P6 space, CL nucleus (red), MD (green), VPL (purple) Cm (cyan). DBS activation of fibers (red), inactive fibers rendered in blue.

B. Histograms of fiber activation for left sided CL. MD, VPL, and Cm.

C. DBS activation of fibers (red), inactive fibers rendered in blue.

D. Active contact locations and fiber bundles for right hemisphere of P6 rendered within P6 space, CL nucleus (red), MD (green), VPL (purple) Cm (cyan).

E. Histograms of fiber activation for right sided CL. MD, VPL, and Cm.

F. DBS activation of fibers (red), inactive fibers rendered in blue.

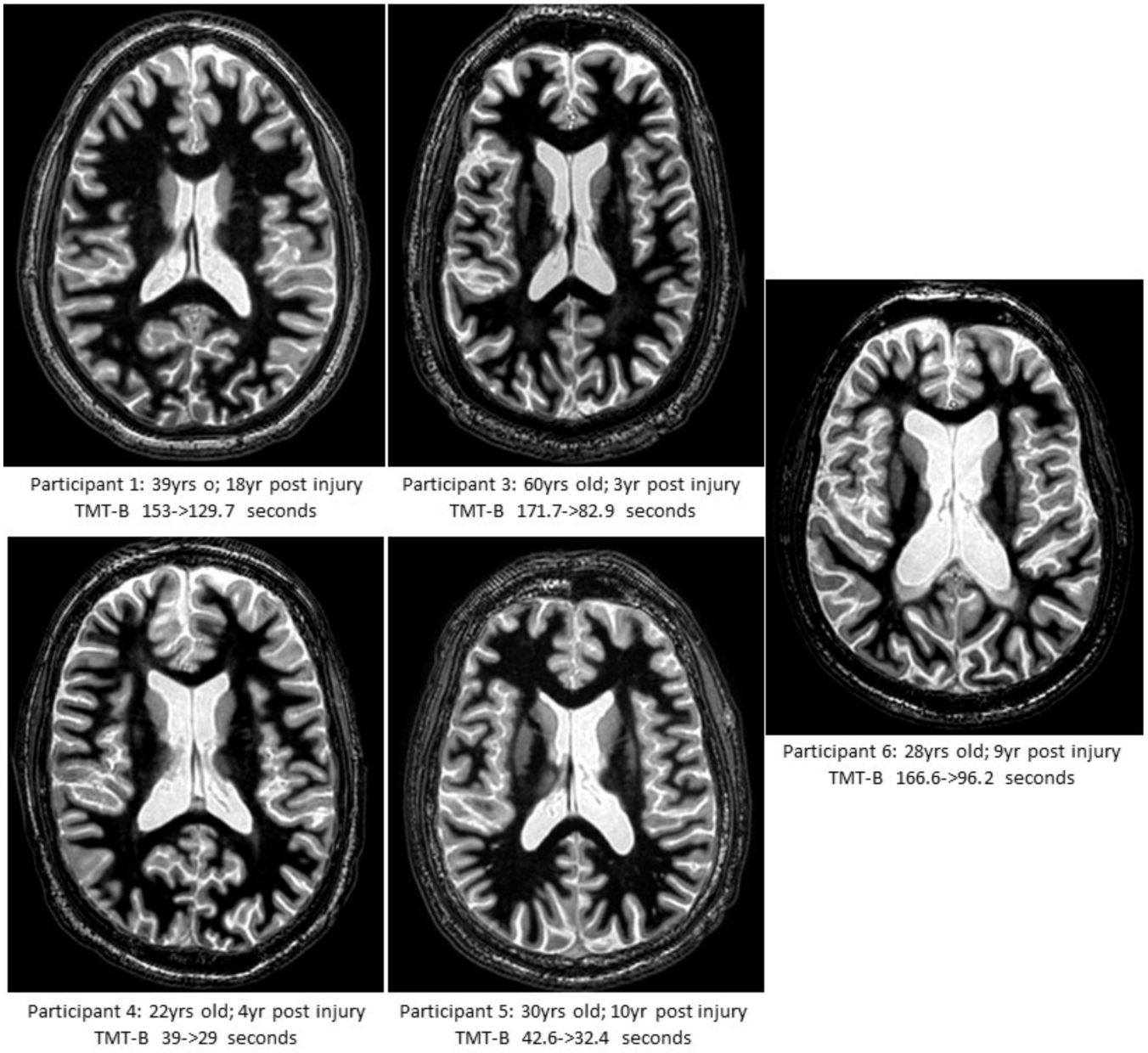

Extended Figure 7. Structural MRI imaging overview all 5 subjects.

Figure shows representative horizontal MRI image from each participant along with demographic information and change in TMT-B performance from pre-surgical to treatment end timepoint.

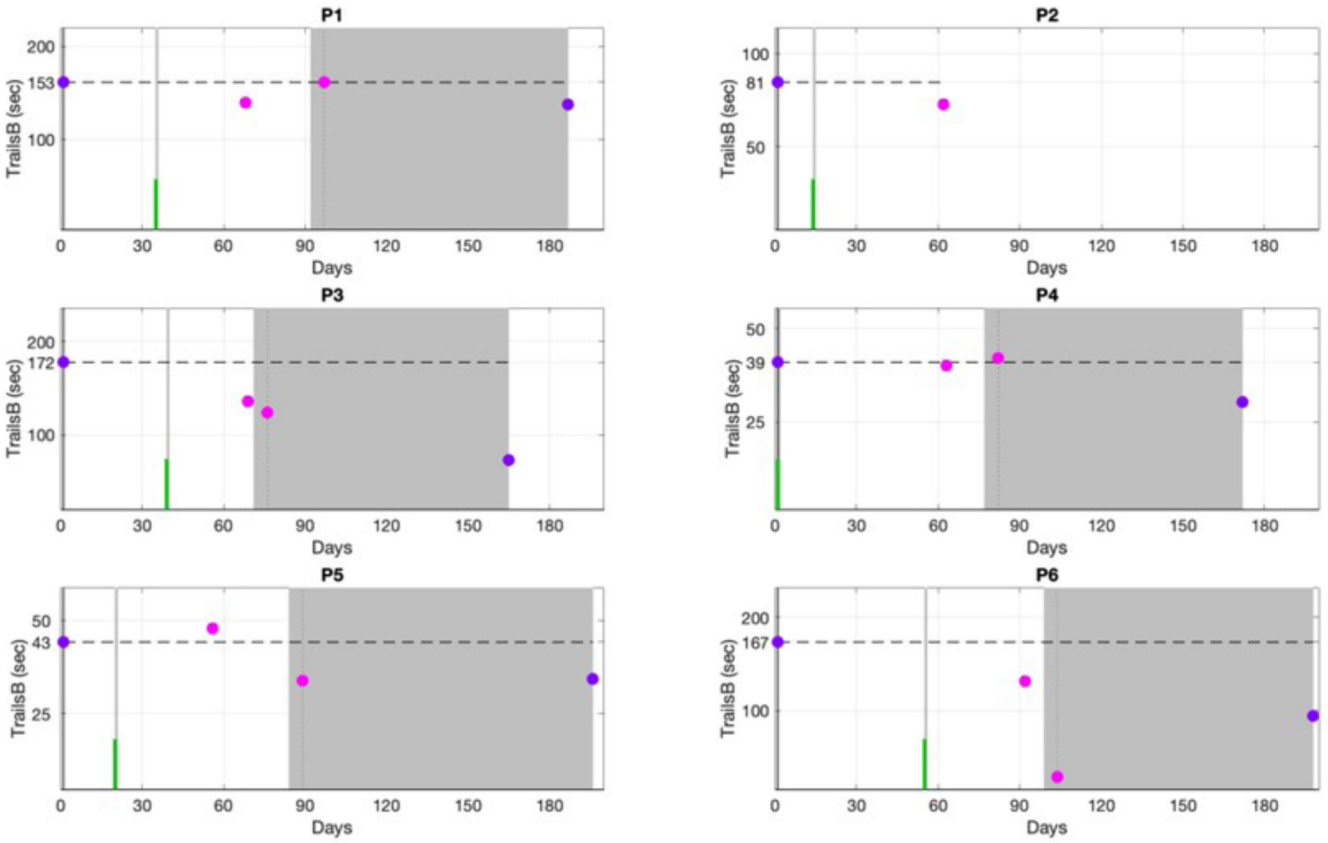

Extended Figure 8: TMT-B completion time measurements across trial phases (all participants). TMT-B completion time raw scores obtained from each participant across each phase of the study. Four timepoints are shown for all participants except for P2 who was withdrawn before initiating the titration phase. The two intermediate time points between pre-surgical baseline (first timepoint, Day 0 all participants) and treatment end measurements reflect many sources of inter-participant variation in times of measurements after surgery, surgical procedures (see Supplemental Methods, Surgical targeting and implantation) and hours of exposure to stimulation prior to "Treatment Start" TMT-B completion time measurement (see Supplemental MethodsTitration Phase and Study design considerations). Exposure to stimulation is indicated by shaded grey regions and includes a brief exposure to stimulation at the time of surgery (green marker on grey bar). The range of separation for the 4 time points across participants varied: Baseline to Post-Surgery (range 55–91 days), Post-Surgery to Treatment Start (7–33 days) and Treatment Start to Treatment End (89–107 days). Abrupt changes with initial exposure to continuous DBS were evident in P3, P5, and P6.

Extended Table 1.

Trial-Making-Test and Cognitive Self-Report Measure Results.

Participant	1	3	4	5	6	Mean
TMT--Raw Scores						
Part B						

Participant	1	3	4	5	6	Mean
Pre-Surgery baseline	153.0	171.7	39.0	42.6	166.6	114.6
Treatment End	129.7	82.9	29.0	32.4	96.2	74.0
Percent Change	**−15.2**	**−51.7**	**−25.6**	**−23.9**	**−42.3**	**−31.7**
Part A						
Pre-Surgery baseline	62.0	85.9	22.1	|18.7	61.6	50.1
Treatment End	41.5	45.9	16.5	14.7	44.7	32.7
Percent Change	**−33.1**	**−46.6**	**−25.3**	**−21.4**	**−27.4**	**−30.8**
TMT--Demographically Adjusted T-Scores:						
Part B						
Pre-Surgery baseline	22	33	62	62	22	40.2
Treatment End	22	50	71	71	35	49.8
Change over time:	**0**	**17**	**9**	**9**	**13**	**9.6**
Part A						
Pre-Surgery baseline	21	20	49	57	22	33.8
Treatment End	30	38	66	71	31	47.2
Change over time:	**9**	**18**	**17**	**14**	**9**	**13.4**
QoL Attention						
Pre-Surgery baseline	19	6	14	10	14	12.6
Treatment End	30	10	21	23	27	22.2
Percent Change	**58**	**67**	**50**	**130**	**93**	**79.6**
QoL Executive Function						
Pre-Surgery baseline	36	20	25	28	24	26.6
Treatment End	43	20	32	43	39	35.4
Percent Change	19	0	28	54	63	**32.8**

Table shows pre- and post-trial results of TMT and related TBI-Qol Attention and Executive function self-report measures for each participant.

Extended Table 2:

Localization of active contacts within synthetic atlas, means and variances.

	Left Lead Active Contact Coordinates			
Patient ID	**Active Contact**	**R/L Coordinate**	**A/P Coordinate**	**S/I Coordinate**
P1	L4	−13 90	4.32	9.62
	L3	−13.10	−5.85	7.00
P3	L4	−13.50	−3.90	8.80
	L3	−12.85	−5.10	6.00
P4	L4	−11.80	−5.20	6.80
	L3	−11.65	−7.10	4.10
	L2*	−11.30	−8.60	1.90
P5	L4	−13.05	−6.60	8.25
	L3	−12.45	−8.20	5.85

Left Lead Active Contact Coordinates				
Patient ID	**Active Contact**	**R/L Coordinate**	**A/P Coordinate**	**S/I Coordinate**
P6	L4	−11.10	−5.40	7.90
	L3	−10.70	−7.10	5.80
	Top Active Contact: Mean	−12.67	−5.08	8.27
	Top Active Contact: Standard Deviation	*1.18*	*1.05*	*1.05*
	Bottom Active Contact: Mean	−12.15	−6.67	5.75
	Bottom Active Contact: Standard Deviation	*0.98*	*1.21*	*1.04*

Right Lead Active Contact Coordinates				
Patient ID	**Active Contact**	**R/L Coordinate**	**A/P Coordinate**	**S/I Coordinate**
P1	R4	8.60	4.10	8.20
	R3	8.10	−5.10	5.40
P3	R4	7.40	4.85	6.85
	R3	7.00	−6.10	4.40
P4	R4	7.40	−2.10	9.70
	R3	7.00	−3.60	7.50
	R2*	6.40	−5.10	4.70
P5	R4	8.60	4.10	9.40
	R3	8.10	−5.70	7.05
P6	R4	8.60	−6.50	8.55
	R3	9.00	−8.50	6.35
	R2	9.40	−10.35	4.00
	Top Active Contact: Mean	8.30	4.89	8.25
	Top Active Contact: Standard Deviation	*0.60*	*1.13*	*1.06*
	Bottoni Active Contact: Mean	7.84	−5.80	6.14
	Bottoni Active Contact: Standard Deviation	*0.85*	*1.78*	*1.25*

Note, for contact R4 position numbers greyed out to reflect shorted contact.

Supplementary Material

Refer to Web version on PubMed Central for supplementary material.

Acknowledgments

Surgical implants (including leads and implantable neurostimulators) were provided by Medtronic. This work was supported by the NIH BRAIN Initiative NINDS grant UH3 NS095554 (NS, JT, CB, EC, JB, KO, AJ, MB, LD, AF, LG, JM, MR, SS, JS, AW, SK, JF, AM,BR,JH). Jason Chua, MPH and Dr. Linda Gerber were partially supported by the following grant: Clinical and Translational Science Center at Weill Cornell Medical College (1-UL1-TR002384-01). The content is solely the responsibility of the authors and does not necessarily represent the official views of the National Institutes of Health (NIH). We thank the following personnel who have supported

this study: Sabrina Taylor (Harvard/Spaulding); Jesse Lee (Weill Cornell); Thomas Prieto, Harvey Fortune, Paymon Rezaii, Omar Rutledge, Anthony Bet, Hong-Bo Yeh, Guiping Qin, Harvey Fortune, Traci Hornbeck, Erika Lim (Stanford); Scott Stanslaski, Caleb Zarns, Natasha Hopps, Paul Stypulkowski (Medtronic, Inc.); Irina Korytov (Utah/Florida); Devi Heyer (PatientWing, Inc. Philadelphia, PA); Biologics Consulting Group, Alexandria, VA. We are grateful to the following: Sarah Hwang for providing the artwork for Supplementary Figure 1; Dr. Ludvik Alkhoury for assistance with Extended FIgure 8; Drs. Grant Iverson and Chad Gaudet for discussion of practice effects in neuropsychological testing; Dr. John Whyte for comments on the manuscript.

References

1. Hammond FM, et al. Patterns of Functional Change Five to Ten Years after Moderate-Severe Traumatic Brain Injury. J Neurotrauma 38, 1526–1534 (2021). [PubMed: 33779295]
2. Wilson L, et al. The chronic and evolving neurological consequences of traumatic brain injury. Lancet Neurol 16, 813–825 (2017). [PubMed: 28920887]
3. Finnanger TG, et al. Life after Adolescent and Adult Moderate and Severe Traumatic Brain Injury: Self-Reported Executive, Emotional, and Behavioural Function 2–5 Years after Injury. Behav Neurol 2015, 329241 (2015).
4. Olsen A, et al. Altered Cognitive Control Activations after Moderate-to-Severe Traumatic Brain Injury and Their Relationship to Injury Severity and Everyday-Life Function. Cereb Cortex 25, 2170–2180 (2015). [PubMed: 24557637]
5. Dikmen SS, Machamer JE, Powell JM & Temkin NR Outcome 3 to 5 years after moderate to severe traumatic brain injury. Arch Phys Med Rehabil 84, 1449–1457 (2003). [PubMed: 14586911]
6. Dikmen SS, et al. Cognitive outcome following traumatic brain injury. J Head Trauma Rehabil 24, 430–438 (2009). [PubMed: 19940676]
7. Draper K. & Ponsford J. Cognitive functioning ten years following traumatic brain injury and rehabilitation. Neuropsychology 22, 618–625 (2008). [PubMed: 18763881]
8. Ruttan L, Martin K, Liu A, Colella B. & Green RE Long-term cognitive outcome in moderate to severe traumatic brain injury: a meta-analysis examining timed and untimed tests at 1 and 4.5 or more years after injury. Arch Phys Med Rehabil 89, S69–76 (2008). [PubMed: 19081444]
9. Lange RT, Iverson GL, Zakrzewski MJ, Ethel-King PE & Franzen MD Interpreting the trail making test following traumatic brain injury: comparison of traditional time scores and derived indices. J Clin Exp Neuropsychol 27, 897–906 (2005). [PubMed: 16183622]
10. Corrigan JD, et al. US population estimates of health and social outcomes 5 years after rehabilitation for traumatic brain injury. J Head Trauma Rehabil 29, E1–9 (2014).
11. in Traumatic Brain Injury: A Roadmap for Accelerating Progress (eds. Matney C, Bowman K. & Berwick D) (Washington (DC), 2022).
12. Tso S, Saha A. & Cusimano MD The Traumatic Brain Injury Model Systems National Database: A Review of Published Research. Neurotrauma Rep 2, 149–164 (2021). [PubMed: 34223550]
13. Iverson GL, Karr JE, Gardner AJ, Silverberg ND & Terry DP Results of scoping review do not support mild traumatic brain injury being associated with a high incidence of chronic cognitive impairment: Commentary on McInnes et al. 2017. PLoS One 14, e0218997 (2019).
14. De Simoni S, et al. Altered caudate connectivity is associated with executive dysfunction after traumatic brain injury. Brain 141, 148–164 (2018). [PubMed: 29186356]
15. Leunissen I, et al. Task switching in traumatic brain injury relates to cortico-subcortical integrity. Hum Brain Mapp 35, 2459–2469 (2014). [PubMed: 23913872]
16. Leunissen I, et al. Subcortical volume analysis in traumatic brain injury: the importance of the fronto-striato-thalamic circuit in task switching. Cortex 51, 67–81 (2014). [PubMed: 24290948]
17. Little DM, et al. Thalamic integrity underlies executive dysfunction in traumatic brain injury. Neurology 74, 558–564 (2010). [PubMed: 20089945]
18. Lutkenhoff ES, et al. The subcortical basis of outcome and cognitive impairment in TBI: A longitudinal cohort study. Neurology 95, e2398–e2408 (2020). [PubMed: 32907958]
19. Baker JL, et al. Robust modulation of arousal regulation, performance, and frontostriatal activity through central thalamic deep brain stimulation in healthy nonhuman primates. J Neurophysiol 116, 2383–2404 (2016). [PubMed: 27582298]

20. Redinbaugh MJ, et al. Thalamus Modulates Consciousness via Layer-Specific Control of Cortex. Neuron 106, 66–75 e12 (2020). [PubMed: 32053769]
21. Deschenes M, Bourassa J. & Parent A. Striatal and cortical projections of single neurons from the central lateral thalamic nucleus in the rat. Neuroscience 72, 679–687 (1996). [PubMed: 9157314]
22. Ellender TJ, Harwood J, Kosillo P, Capogna M. & Bolam JP Heterogeneous properties of central lateral and parafascicular thalamic synapses in the striatum. J Physiol 591, 257–272 (2013). [PubMed: 23109111]
23. Llinas RR, Leznik E. & Urbano FJ Temporal binding via cortical coincidence detection of specific and nonspecific thalamocortical inputs: a voltage-dependent dye-imaging study in mouse brain slices. Proc Natl Acad Sci U S A 99, 449–454 (2002). [PubMed: 11773628]
24. Shirvalkar P, Seth M, Schiff ND & Herrera DG Cognitive enhancement with central thalamic electrical stimulation. Proc Natl Acad Sci U S A 103, 17007–17012 (2006). [PubMed: 17065322]
25. Liu J, et al. Frequency-selective control of cortical and subcortical networks by central thalamus. Elife 4, e09215 (2015). [PubMed: 26652162]
26. Wyder MT, Massoglia DP & Stanford TR Contextual modulation of central thalamic delay-period activity: representation of visual and saccadic goals. J Neurophysiol 91, 2628–2648 (2004). [PubMed: 14762161]
27. Schiff ND Recovery of consciousness after brain injury: a mesocircuit hypothesis. Trends Neurosci 33, 1–9 (2010). [PubMed: 19954851]
28. Schiff ND, et al. Behavioural improvements with thalamic stimulation after severe traumatic brain injury. Nature 448, 600–603 (2007). [PubMed: 17671503]
29. Janson AP, et al. Selective activation of central thalamic fiber pathway facilitates behavioral performance in healthy non-human primates. Sci Rep 11, 23054 (2021). [PubMed: 34845232]
30. Edlow BL, et al. Neuroanatomic connectivity of the human ascending arousal system critical to consciousness and its disorders. J Neuropathol Exp Neurol 71, 531–546 (2012). [PubMed: 22592840]
31. Janson AP & Butson CR Targeting Neuronal Fiber Tracts for Deep Brain Stimulation Therapy Using Interactive, Patient-Specific Models. J Vis Exp (2018).
32. Lannoo E, Colardyn F, Jannes C. & de Soete G. Course of neuropsychological recovery from moderate-to-severe head injury: a 2-year follow-up. Brain Inj 15, 1–13 (2001). [PubMed: 11201310]
33. Wilson L, et al. A Manual for the Glasgow Outcome Scale-Extended Interview. J Neurotrauma 38, 2435–2446 (2021). [PubMed: 33740873]
34. Sanchez-Cubillo I, et al. Construct validity of the Trail Making Test: role of task-switching, working memory, inhibition/interference control, and visuomotor abilities. J Int Neuropsychol Soc 15, 438–450 (2009). [PubMed: 19402930]
35. Heaton RK, Walden Miller S, Taylor MJ & Grant I. Revised Comprehensive Norms for an Expanded Halstead-Reitan Battery: Demographically Adjusted Neuropsychological Norms for African American and Caucasian Adults. in Psychological Assessment Resources (Odessa, FL, 2004).
36. Fins JJ, Wright MS, Henderson JM & Schiff ND Subject and Family Perspectives from the Central Thalamic Deep Brain Stimulation for Traumatic Brain Injury Study: Part I. Camb Q Healthc Ethics 31, 419–443 (2022). [PubMed: 36398511]
37. Fins JJ, Wright MS, Shulman KS, Henderson JM & Schiff N. Subject and Family Perspectives from the Central Thalamic Deep Brain Stimulation for Traumatic Brain Injury Study: Part II. Camb Q Healthc Ethics In Press(2023).
38. Hart T, Whyte J, Kim J. & Vaccaro M. Executive function and self-awareness of “real-world” behavior and attention deficits following traumatic brain injury. J Head Trauma Rehabil 20, 333–347 (2005). [PubMed: 16030440]
39. Hsu DT & Price JL Midline and intralaminar thalamic connections with the orbital and medial prefrontal networks in macaque monkeys. J Comp Neurol 504, 89–111 (2007). [PubMed: 17626282]

40. Morel A, Liu J, Wannier T, Jeanmonod D. & Rouiller EM Divergence and convergence of thalamocortical projections to premotor and supplementary motor cortex: a multiple tracing study in the macaque monkey. Eur J Neurosci 21, 1007–1029 (2005). [PubMed: 15787707]
41. Shook BL, Schlag-Rey M. & Schlag J. Primate supplementary eye field. II. Comparative aspects of connections with the thalamus, corpus striatum, and related forebrain nuclei. J Comp Neurol 307, 562–583 (1991). [PubMed: 1869632]
42. Steriade M. & Glenn LL Neocortical and caudate projections of intralaminar thalamic neurons and their synaptic excitation from midbrain reticular core. J Neurophysiol 48, 352–371 (1982). [PubMed: 6288887]
43. Bastos AM, et al. Neural effects of propofol-induced unconsciousness and its reversal using thalamic stimulation. Elife 10(2021).
44. Tasserie J, et al. Deep brain stimulation of the thalamus restores signatures of consciousness in a nonhuman primate model. Sci Adv 8, eabl5547 (2022).
45. Steriade M. Neocortical neurons are flexible entities. Trends in Neuroscience 5, 121–134 (2004).
46. Rudolph M, Pelletier JG, Pare D. & Destexhe A. Characterization of synaptic conductances and integrative properties during electrically induced EEG-activated states in neocortical neurons in vivo. J Neurophysiol 94, 2805–2821 (2005). [PubMed: 16014785]
47. Bernander O, Douglas RJ, Martin KA & Koch C. Synaptic background activity influences spatiotemporal integration in single pyramidal cells. Proc Natl Acad Sci U S A 88, 11569–11573 (1991). [PubMed: 1763072]
48. Larkum ME, Zhu JJ & Sakmann B. A new cellular mechanism for coupling inputs arriving at different cortical layers. Nature 398, 338–341 (1999). [PubMed: 10192334]
49. Larkum ME, Waters J, Sakmann B. & Helmchen F. Dendritic spikes in apical dendrites of neocortical layer 2/3 pyramidal neurons. J Neurosci 27, 8999–9008 (2007). [PubMed: 17715337]
50. Khubieh A, Ratte S, Lankarany M. & Prescott SA Regulation of Cortical Dynamic Range by Background Synaptic Noise and Feedforward Inhibition. Cereb Cortex 26, 3357–3369 (2016). [PubMed: 26209846]
51. Shu Y, Hasenstaub A, Badoual M, Bal T. & McCormick DA Barrages of synaptic activity control the gain and sensitivity of cortical neurons. J Neurosci 23, 10388–10401 (2003). [PubMed: 14614098]
52. Baker JL, et al. Central thalamic deep brain stimulation enhances dominant spiking activity profiles of prefrontal and premotor cortical neurons in healthy and behaving non-human primates. in 5th Annual Minnesota Neuromodulation Symposium (2018).
53. Kang Y, et al. Longitudinal alterations in gamma-aminobutyric acid (GABA(A)) receptor availability over approximately 1 year following traumatic brain injury. Brain Commun 4, fcac159 (2022).
54. Laureys S. & Schiff ND Coma and consciousness: paradigms (re)framed by neuroimaging. Neuroimage 61, 478–491 (2012). [PubMed: 22227888]
55. Schiff ND, Purpura KP & Victor JD Gating of local network signals appears as stimulus-dependent activity envelopes in striate cortex. J Neurophysiol 82, 2182–2196 (1999). [PubMed: 10561398]
56. Purpura KP & Schiff ND The thalamic intralaminar nuclei: A role in visual awareness. Neuroscientist 3, 8–15 (1997).
57. Mair RG & Hembrook JR Memory enhancement with event-related stimulation of the rostral intralaminar thalamic nuclei. J Neurosci 28, 14293–14300 (2008). [PubMed: 19109510]
58. Tabansky I, et al. Temporally-patterned deep brain stimulation in a mouse model of multiple traumatic brain injury. Behav Brain Res 273, 123–132 (2014). [PubMed: 25072520]
59. Fins JJ A proposed ethical framework for interventional cognitive neuroscience: a consideration of deep brain stimulation in impaired consciousness. Neurol Res 22, 273–278 (2000). [PubMed: 10769820]
60. Shah SA, Baker JL, Ryou JW, Purpura KP & Schiff ND Modulation of arousal regulation with central thalamic deep brain stimulation. Ieee Eng Med Bio, 3314–3317 (2009).
61. Smith AC, et al. A Bayesian statistical analysis of behavioral facilitation associated with deep brain stimulation. J Neurosci Meth 183, 267–276 (2009).

62. Su JH, et al. Thalamus Optimized Multi Atlas Segmentation (THOMAS): fast, fully automated segmentation of thalamic nuclei from structural MRI. Neuroimage 194, 272–282 (2019). [PubMed: 30894331]

63. Mukherjee A, Lam NH, Wimmer RD & Halassa MM Thalamic circuits for independent control of prefrontal signal and noise. Nature 600, 100–104 (2021). [PubMed: 34614503]

64. Bigdely-Shamlo N, Mullen T, Kothe C, Su KM & Robbins KA The PREP pipeline: standardized preprocessing for large-scale EEG analysis. Front Neuroinform 9, 16 (2015). [PubMed: 26150785]

65. Bell AJ & Sejnowski TJ An information-maximization approach to blind separation and blind deconvolution. Neural Comput 7, 1129–1159 (1995). [PubMed: 7584893]

66. Baker KB, Montgomery EB Jr., Rezai AR, Burgess R. & Luders HO Subthalamic nucleus deep brain stimulus evoked potentials: physiological and therapeutic implications. Mov Disord 17, 969–983 (2002). [PubMed: 12360546]

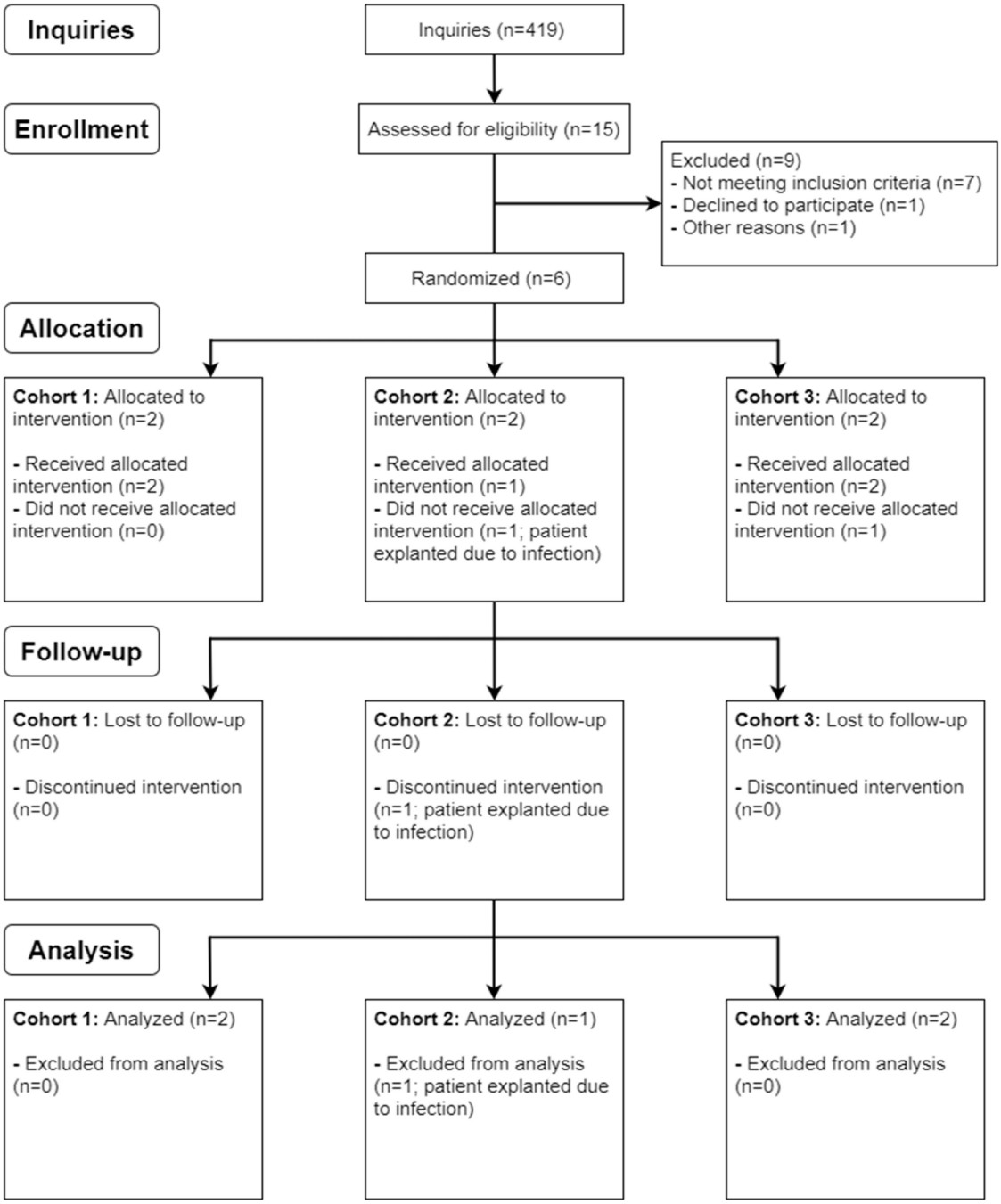

Figure 1.
CONSORT Diagram

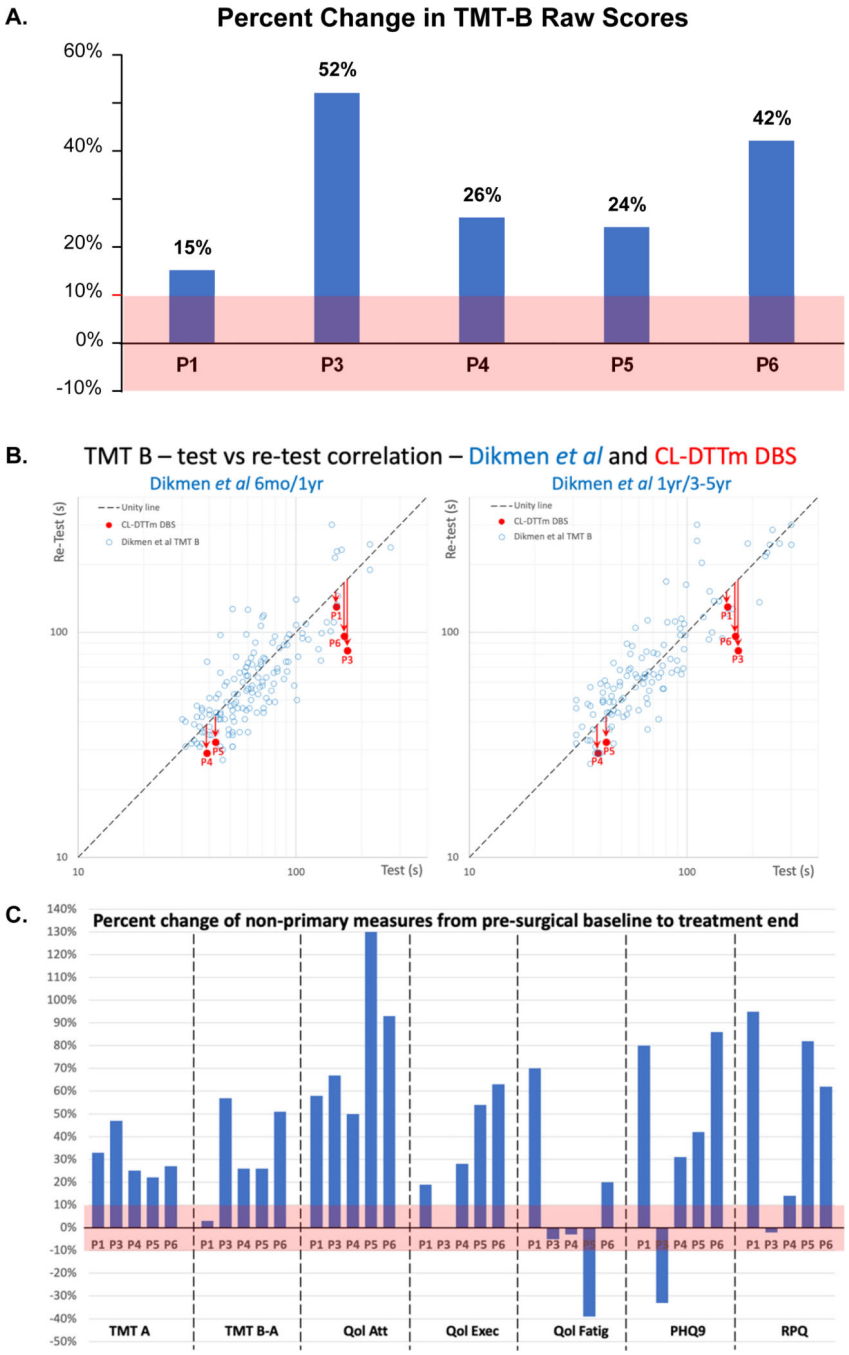

Figure 2. Behavioral results.

A. TMT-B raw scores for each subject. Red line indicates 10% improvement level, the pre-selected benchmark.

B. Test-retest scattergram. Scattergram of data from two groups of msTBI subjects (blue dots) followed as part of the Dikmen et al.[5] study with available TMT-B measurements at time points: 1) (n=146) 6 months post-injury and again 1 year post-injury, and 2) (n= 118) who were followed 1 year post-injury and again between 3 and to 5 years post-injury (provided by Dr. Dikmen) together with the five msTBI participants studied

here (red dots). The CL/DTTm subjects cluster on the lower edge of the “natural recovery” group distributions. Statistical tests demonstrate that it is unlikely that the CL/DTTm DBS participant values have been drawn from either of the “natural recovery” distributions: A) $p<0.02$ Kolmogorov-Smirnov test, one-sided [$p=0.011$], B) $p<0.005$ Kolmogorov-Smirnov, one-sided [0.004070].

C. Percent change of non-primary measures from pre-surgical baseline to treatment end. All non-primary measures obtained across all 5 participants completing the study are shown. Improvement on measure is indicated by positive change in percentage, worsening is indicated by a negative change in percentage (see Supplemental Material). For Ruff 2&7 measures complete pre-surgical data were only available for 4 subjects (see Supplementary Table 1).

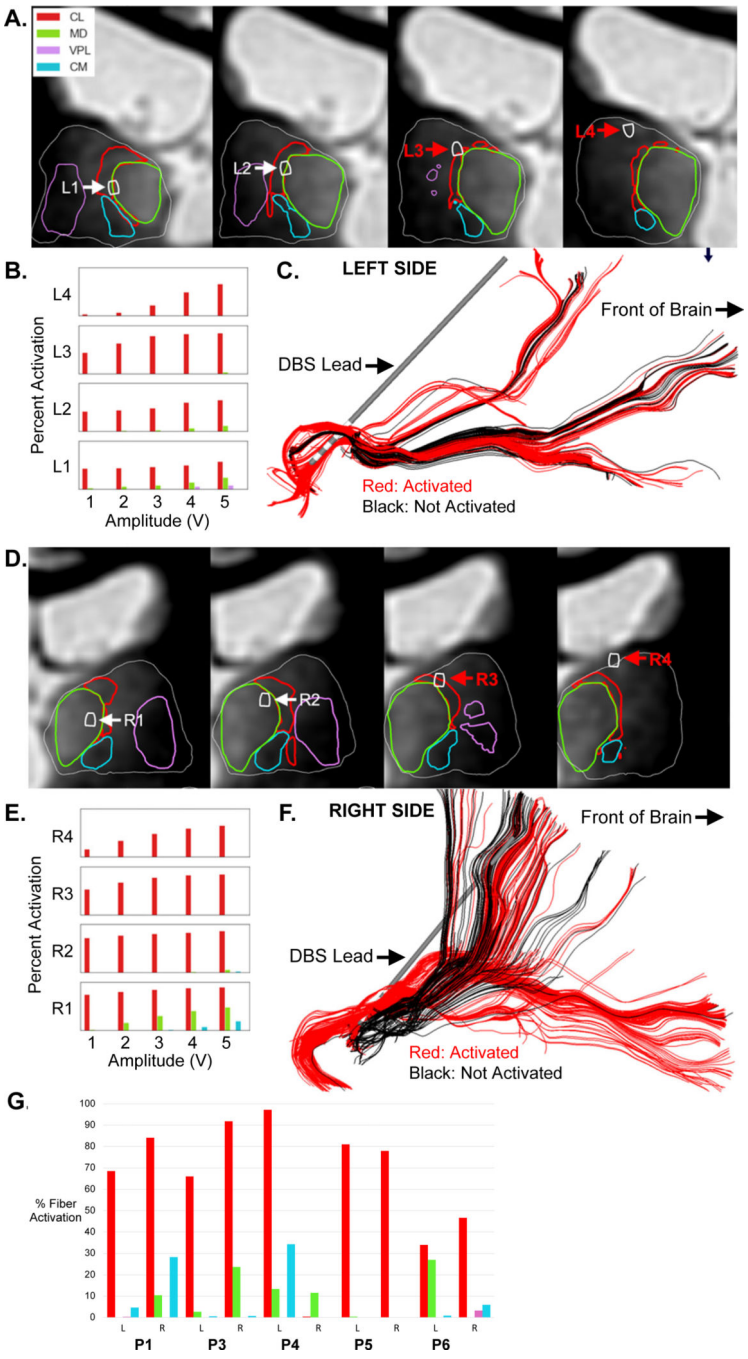

Figure 3. Activation of CL/DTTm fibers in a representative subject and group summary.

A. Coronal WMn slices from left hemisphere of participant P5, zoomed to include only left thalamus and lateral ventricle. Four slices are shown: each intersects the middle of one of the four DBS electrode contacts. The two active contacts L3 and L4 (used as cathodes during stimulation) are indicated by red labels and arrows. The intersection of each slice with the outer boundary of four “key” thalamic nuclei are indicated by the color contours: CL (red), MD (green), VPL (purple), Cm (cyan).

B. Histograms of fiber activation from left hemisphere of participant P5, for each of the four DBS contacts driven at five different voltages from 1V to 5V, for CL, MD, VPL, and Cm fibers.

C. Modeled activation of P5's left hemisphere CL/DTTm fibers (active fibers rendered in red, inactive fibers rendered in blue).

D. Coronal WMn slices from right hemisphere of participant P5, zoomed to include only right thalamus and lateral ventricle. Four slices are shown: each intersects the middle of one of the four DBS electrode contacts. The two active electrode contacts R3 and R4 (used as cathodes during stimulation) are indicated by red labels and arrows. The intersection of each slice with the outer boundary of four "key" thalamic nuclei are indicated by the color contours: CL (red), MD (green), VPL (purple), Cm (cyan).

E. Histograms of modeled fiber activation from right hemisphere of participant P5, for each of the four DBS electrode contacts driven at five different voltages from 1V to 5V, for CL, MD, VPL, and Cm fibers.

F. Modeled activation of P5's right hemisphere CL/DTTm fibers (active fibers rendered in red, inactive fibers rendered in black).

G. Percent of fiber activation of target and avoidance fibers, all five participants. Color scheme is the same as in panels A, B, D, E: CL (red), MD (green), VPL (purple), Cm (cyan).

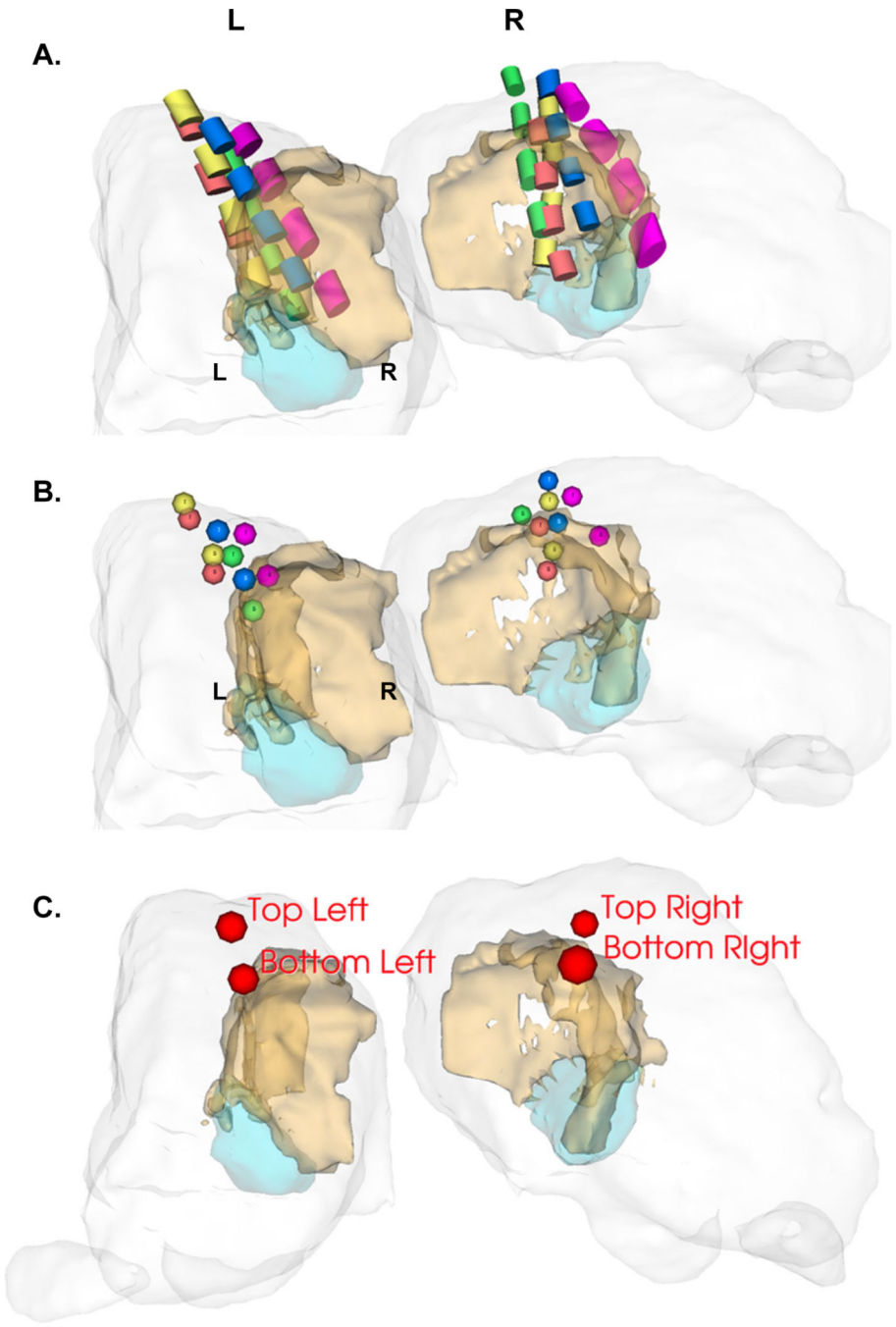

Figure 4. Placement and visualization of DBS contacts in common template space.

A. CL and Cm. 3D rendering of CL (light brown) and Cm (cyan) nuclei within the thalamus (transparent grey). **Post-op electrodes.** Rendering of the four DBS electrodes for each of the five participants, color-coded by participant as follows: P1 (yellow), P3 (salmon), P4 (green), P5 (blue), P6 (magenta). These electrode renderings indicate the final post-operative locations, as determined by 30-day post-operative CT scanning, and like all other panels in this figure, these locations have been warped into common template space.

B. Active contacts identified. Small spherical renderings are shown within two of the DBS electrodes on each of left and right sides, to indicate that these are the two (top and bottom) active contacts used during stimulation of this participant. Note that the top active contact on the right side for P4 (green) was shorted as a result of this contact being fully outside the thalamus and in the CSF of the lateral ventricle. For this reason this contact could not be used during stimulation and is therefore not shown in this panel, nor was it used for the computation of centroids.

C. Active contact centroid spheres. Centroids of top and bottom contacts computed across the five participants, and rendered as red spheres, with location of the sphere showing the 3D location of the centroid and the diameter of the sphere set equal to the standard deviation (spatial spread) across the five participants, providing a graphical indication of the tightness-of-clustering of top and bottom active contacts in common space, in relation to CL and outer surface of thalamus.

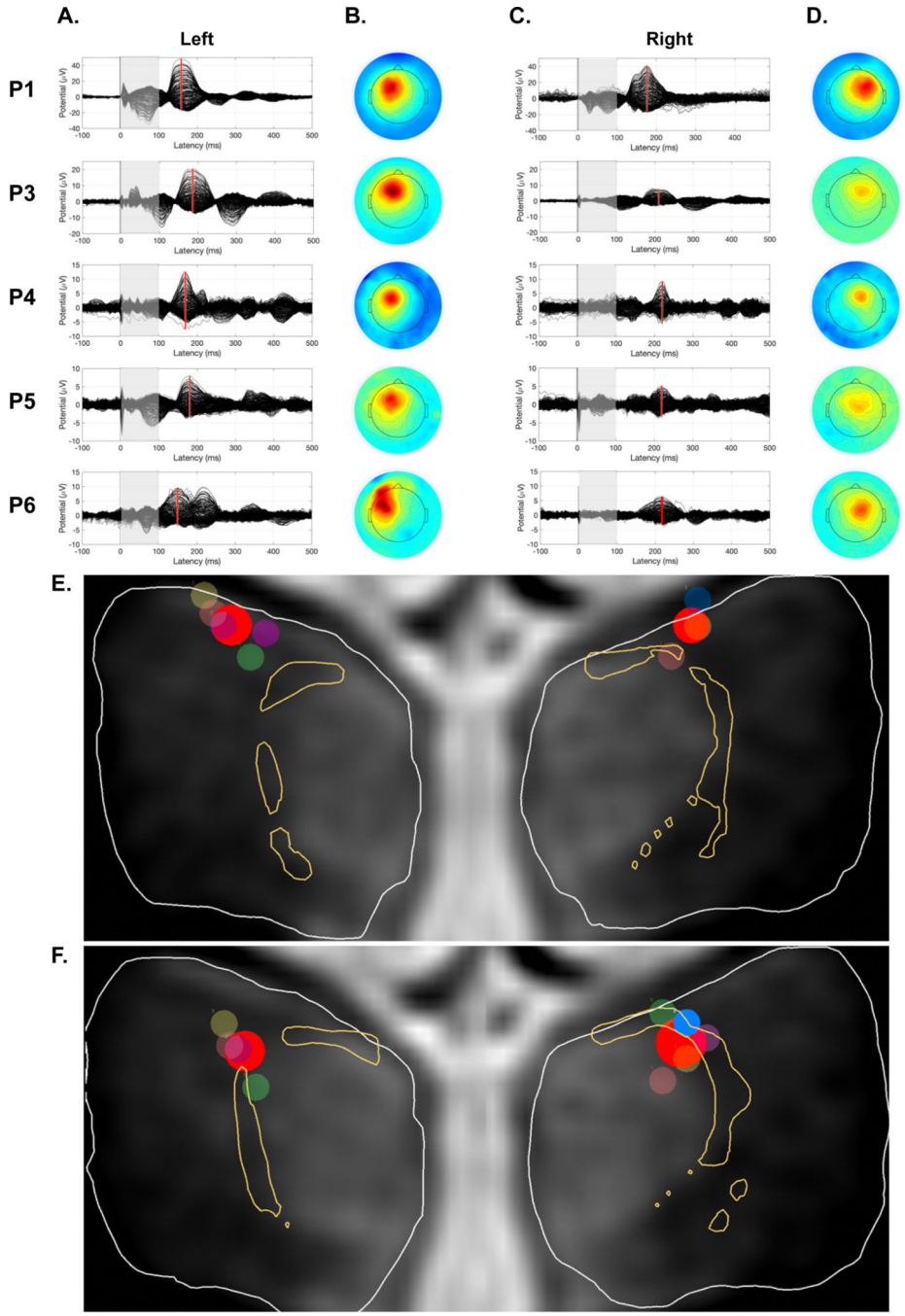

Figure 5. Cortical evoked responses for each individual subject from left and right hemisphere.

Top panels (A-D). DBS-evoked potentials obtained for the therapeutic contacts selected during the titration phase for treatment DBS for each subject (see also Supplementary Figures 2–11). Stimulation was applied for the first 100ms Robust evoked potentials localized to the ipsilateral frontal cortex, with a peak amplitude between medial and lateral regions of frontal cortex is noted in each panel. This is consistent with animal anatomical literature showing CL's strong connectivity to the dorsomedial frontal cortex[39,40]. Evoked potentials in the left hemisphere demonstrate greater inter-subject consistency than those in

the right hemisphere. As shown below (and see Figure 4, Extended Table 2), right sided bottom active contacts demonstrate greater variance in location potentially influencing this greater right-sided variability.

Bottom panels (E, F). Coronal slices through the common template WMn volume, zoomed to show thalamus and mid-line CSF only. Thin boundaries indicate the Intersection of each slice with the THOMAS segmentations for CL (light brown) and whole thalamus (white). Small circles show the active contacts, color-coded for each participant similarly to those shown in Figure 4, rendered as dim if out-of-plane or bright if in-plane. Bright red larger circles indicate the intersection between the centroid spheres and the slice plane, with top active contacts and centroids shown in panel E and bottom active contacts and centroids shown in panel F.

Table 1.

Patient Demographics Table

Sample Characteristics							
Participant	**1**	**2**	**3**	**4**	**5**	**6**	**Mean**
Demographics							
Age	39	38	60	22	30	28	36.2
Yrs since Injury	18	2	3	4	10	9	7.7
Yrs Education	16	14	13	13	14	14	14
Gender	F	F	M	M	M	M	
Injury Characteristics							
Prior TBI	N	N	Y	N	N	N	
Cause of injury	MVA	MVA	Fall[^]	MVA [*]	MVA	Fall[^^]	
Highest level of care	ICU	ER	ICU	ICU	ICU	ICU	
Loss of consciousness	Y	Y	Y	Y	Y	Y	
GOS-E pre-surgery	5	5	5	5	6	6	
Return to prior employment/academic level (Yes/No)	No	No	No	No	No	No	
Self-Reported Symptoms (+ Present / - Absent)							
Cognitive-Behaviioral							
Hypoarousal / lethargy / somnolence	-	-	-	+	+	-	
Fatigue	+	+	+	+	+	-	
Insomnia / sleep disturbance	-	+	-	+	+	-	
Confusion	-	+	+	+	-	-	
Thinking abnormality	-	-	-	-	-	+	
Attention impairment	+	-	+	+	+	-	
Memory impairment / amnesia	+	+	+	+	+	+	
Language impairment	+	-	-	+	+	-	
Slurred speech	-	+	-	+	-	-	
Executive function impairment	+	+	-	+	+	-	
Motor restlessness / hyperkinesia	+	+	-	+	-	-	
Agitation/aggression	+	+	-	-	+	-	
Irritability	+	+	-	+	+	-	
Nervousness	+	+	-	-	+	-	
Depression	+	+	+	-	+	-	
Anxiety	+	+	+	-	+	-	
Paranoid reaction	-	-	-	-	+	-	
Sensory-Motor							
Decreased visual acuity	-	+	+	-	+	-	
Sensitivity to light	-	+	+	-	+	-	
Dizziness/Lightheadedness	-	+	-	+	+	-	
Weakness	-	-	-	-	+	-	
Involuntary muscle contractions	+	-	-	-	-	-	
Pain							

Sample Characteristics							
Participant	**1**	**2**	**3**	**4**	**5**	**6**	**Mean**
Headaches	+	+	+	+	+	-	
Limb pain	-	-	-	-	+	-	
Abdominal pain	-	-	-	-	+	-	
Chest pain	-	-	-	-	+	-	
General Medical							
Nausea	-	-	-	-	+	-	
Constipation	-	-	-	-	+	-	
Diarrhea	-	-	-	-	+	-	
Dysphagia	+	-	-	-	-	-	
Urinary retention	-	-	-	-	+	-	
Hypertension	-	-	-	-	+	-	
Skin rash	-	-	-	-	-	+	
Pruritis	+	-	-	-	-	+	
Hair loss	-	-	-	-	+	-	
Pre-Surg Test Performance (Executive Measures)							
TMT Completion Time (secs)							
Part A	62	38.7	85.9	22.1	18.7	61.6	48.2
Part B	153.0	80.8	171.7	39.0	42.6	166.6	109.0
TMT-Demographically Adjusted T-Scores:							
Part A	21	32	20	49	57	22	33.5
Part B	22	38	33	62	62	22	39.8
TBI-QoL Atten/Concent v.1 SF6a Total Raw Score	19	12	6	14	10	14	12.5
TBI-QoL Exec Func v.1 SF10a Total Raw Score	36	23	20	25	28	24	26.0

GOS-E: Glasgow Outcome Scale-Extended (Range: 1 [Dead] - 8 [Return to normal life]); TMT: Trail Making Test: (Range: 0 – 300s); TBI-QoL Atte/Concent v. 1 SF6a: Traumatic Brain Injury- Quality of Life Attention and Concentration Version 1.0 6-item Short Form (Range: 6 – 30 - higher scores = greater symptom burden); TBI-QoL Exec Func v.1 SF6a (Traumatic Brain Injury-Quality of Life Executive Function Version 1.0 10-item Short Form (Range: 10 – 50 - higher scores = better performance).

^ Fall from 450 feet

^^ Fall from 5 stories

* Bicyclist hit by motor vehicle.